A Comprehensive Assessment of a new series of 5',6'-difluorobenzotriazole-acrilonitrile derivatives as Microtubule Targeting Agents (MTAs)

Federico Riu [a], Luca Sanna [b], Roberta Ibba [a,*], Sandra Piras [a], Valentina Bordoni [b], M. Andrea Scorciapino [c], Michele Lai [d], Simona Sestito [a], Luigi Bagella [b,e,*], Antonio Carta [a]

[a] *Department of Chemistry and Pharmacy, University of Sassari, via Vienna 2, 07100, Sassari, Italy.*
[b] *Department of Biomedical Sciences, University of Sassari, via Vienna 2, 07100, Sassari, Italy.*
[c] *Department of Chemical and Geological Sciences, University of Cagliari, S.P. 8 km 0.700, 09042, Monserrato (CA), Italy.*
[d] *Retrovirus Centre, Department of Translational Medicine and New Technologies in Medicine and Surgery, University of Pisa, Strada Statale del Brennero, 2, Pisa, Italy.*
[e] *Sbarro Institute for Cancer Research and Molecular Medicine, Center for Biotechnology, College of Science and Technology, Temple University, Philadelphia, PA, USA.*
* *Corresponding authors. Email addresses: ribba@uniss.it (R. Ibba), lbagella@uniss.it (L. Bagella)*

ABSTRACT

Microtubules (MTs) are the principal target for drugs acting against mitosis. These compounds, called microtubule targeting agents (MTAs), cause a mitotic arrest during G2/M phase, subsequently inducing cell apoptosis. MTAs could be categorised in two groups: microtubule stabilising agents (MSAs) and microtubule destabilising agents (MDAs). In this paper we present a new series of (*E*)(*Z*)-2-(5,6-difluoro-(1*H*)2*H*-benzo[*d*][1,2,3]triazol-1(2)-yl)-3-(*R*)acrylonitrile (**9a-j**, **10e**, **11a,b**) and (*E*)-2-(1*H*-benzo[*d*][1,2,3]triazol-1-yl)-3-(*R*)acrylonitrile derivatives (**13d,j**), which were recognised to act as MTAs agents. They were rationally designed, synthesised, characterised and submitted to different biological assessments. Computational docking was employed in order to prove that these molecules were able to bind the colchicine-binding site on tubulin. From this first prediction, the di-fluoro substitution seemed to be beneficial for the binding affinity with tubulin. The new fluorine derivatives, here presented, brought to a better antiproliferative activity when compared to the previously reported compounds. The biological assessment included a first antiproliferative screening on NCI60 cancer cells panel (1-10 μM). Compound **9a** was selected as lead compound of the new series of derivatives. The *in vitro* XTT, flow cytometry assays and immunostaining on HeLa cells confirmed that **9a** is a MDA which operates by inhibiting the polymerisation of tubulin. It results in a considerable increase of the number of cells in G2/M-phase, an increased number of cell division defects and displaying a 50% reduction of alive cells (IC_{50} = 3.2 μM). Then, a co-administration assay was conducted combining compound **9a** and an extrusion pump inhibitor (EPI): this association resulted beneficial for the antiproliferative activity and compound **9a** showed to be client of extrusion pumps. Physicochemical, pharmacokinetic and druglikeness predictions were conducted. All the synthesised derivatives showed to be drug-like molecules.

Keywords: microtubule destabilising agents; benzotriazoles; tubulin; efflux pump inhibition; cell growth inhibition; molecular docking.

1. Introduction

Cancer is one of the noncommunicable diseases (NCDs) and it is expected to become the leading death cause and the principal obstacle for the increase of life expectancy in the 21st century. [1] Deaths caused by cancer represent approximately 22% of all NCD casualties. [2] The actual shortage of efficient and safe drugs functioning in cancer treatment is a driving force for an increase in the research effort in this field. [3] One of the main characteristics of a tumour cell is its uncontrolled division. Cell division cycle is composed of four successive phases called G1 (Gap 1), S (DNA synthesis), G2 (Gap 2), and M (mitosis). Cell cycle phases convey important information regarding the cytotoxic potential of anticancer drugs. [4] A crucial element involved during cell replication is the mitotic spindle, mainly composed of microtubules (MTs). MTs are filaments composed of α- and β-tubulin heterodimers. An attractive approach to be considered during the therapeutic agents design is the interference with the MT dynamic equilibrium. [5–7] A wide variety of drugs that targets mitotic spindle have been investigated. However, little is known about the mechanism of cell death caused by those drugs. Generally, drugs acting against cell division cycle lead to mitotic arrest during G2/M phase, subsequently inducing cell apoptosis. Nowadays, microtubule targeting agents (MTAs) are some of the most effective drugs used in the treatment of both solid and haematological tumours. MTAs could be categorised in two groups: microtubule stabilising agents (MSAs) and microtubule destabilising agents (MDAs). Both types of agents suppress microtubule dynamics during *in vitro* assay. MTAs could also be categorised into 5 classes based on their interactions with the taxane-, vinca-, colchicine-, laulimalide/peloruside- or the maytansine-site on tubulin. Colchicine binding site inhibitors (CBSIs), comprise a variety of small molecules which include colchicine and combretastatins A-1 (CA-1) and A-4 (CA-4), which bind in the colchicine site (CBS) located on β-tubulin at its interface with α-tubulin. [8,9] Combretastatin A-4 phosphate (CA-4P) and A-1 diphosphate (CA-1P), 2-methoxyestradiol and verubulin are some of the colchicine-site binding agents which have been evaluated in phase 1 and 2 clinical trials. [10] Thus far, no colchicine site agent has been approved as anticancer agent. Hence, this site provides new opportunities for drug discovery. [11–13] We already published a group of benzotriazolacrilonitrile derivatives which turned out to be CBSIs. [14–19] All derivatives can be grouped into two chemical classes, 1*H*-benzotriazole derivatives which showed good activity, and the parental 2*H*-benzotriazole derivatives with a weaker antiproliferative activity. [14] Among all synthesised derivatives, (*E*)-2-(1*H*-benzo[*d*][1,2,3]triazol-1-yl)-3-(4-methoxyphenyl)acrylonitrile was identified as lead compound, hereinafter labelled as compound **A**. Cell cycle analysis revealed the mechanism of action for the lead compound; it inhibits the G2/M phase of cell cycle. The combination of experimental and computational results supports the hypothesis that this class of compounds acts as antiproliferative agents by interacting with tubulin in the colchicine-binding site. Therefore, inhibiting the tubulin assembly, they might be classified as MDAs. [17] The introduction of fluorine atoms is widely used in medicinal chemistry to gain better effects on metabolic stability, bioavailability and ligand-protein interactions (by altering the pK_a). [20] Aromatic fluorination can also increase the compound lipophilicity, [21] and can be used to protect some metabolically weak sites (easily affected by the oxidative effect of the Cytochrome P450) on a ligand. [22] This project aimed to keep the benzotriazole-acrylonitrile backbone and functionalise it with two small halogen atoms, such as fluorine, in position 5' and 6' on the benzotriazole moiety. In this paper we present a new series of (*E*)(*Z*)-2-(5,6-difluoro-(1*H*)2*H*-benzo[*d*][1,2,3]triazol-1(2)-yl)-3-(*R*)acrylonitrile (**9a-j**, **10e**, **11a,b**) and (*E*)-2-(1*H*-benzo[*d*][1,2,3]triazol-1-yl)-3-(*R*)acrylonitrile derivatives (**13d,j**), which were rationally designed, synthesised, characterised and submitted to different biological assessments.

2. Results and Discussion

2.1. Molecular Docking

In order to evaluate the feasibility and the benefit of the fluorine substitution on the benzotriazole moiety, molecular docking simulations were performed. Aiming to compare their binding affinity with the tubulin active site, colchicine as a known ligand, compound **A** and the newly designed difluoro-derived parental compound (labelled derivative **9b**) were docked in the colchicine-binding site on tubulin. The X-ray structure of tubulin co-crystallised with colchicine, PDB ID: 4O2B, was selected. Colchicine was removed from its binding pocket in tubulin and re-docked in the same binding pocket with the same coordinates. It resulted in affinity energy of -9.8 kcal/mol. The same protein structure, without colchicine in place, was employed for docking studies on compounds **A** and **9b**. The best-docked pose for **A** presented binding energy of -6.7 kcal/mol, meanwhile the best-docked pose of compound **9b** ranked affinity energy of -8.6 kcal/mol. All dockings were analysed with PyMOL, [23] Maestro [24] and LigPlot. [25] As depicted in Figure 1, **9b** has two F···N electrostatic interactions, better-called fluorine bonds, [26] involving the electron-acceptor fluorine in position 5 on the benzotriazole scaffold (depicted in Figure 1b as green dashes). These dipole-dipole interactions involve intrinsic nitrogen atoms of Cysβ241 and Leuβ242 (~4 Å). Leuβ242 contributes also with hydrophobic interactions between the carbons of the isobutyl side chain of the amino acid (aa) and the benzotriazole carbons. The benzene moiety of the benzotriazole gives hydrophobic interactions with Alaβ250, Aspβ251 and Leuβ255, while the side-chain benzene moiety has van der Waals interactions with aas of the opposite portion of the binding pocket: Leuβ248, Gluα183, Lysβ254 and Asnβ258. The amidic nitrogen atom of Asnα101 interacts with the acceptor oxygen of the methoxyl group of compound **A**, forming a hydrogen bond (4.18 Å, Figure 1a). The best binding pose of **9b**, showed the methoxyl group in a different conformation if compared with **A**, there is only a weak interaction with the same asparagine residue, accordingly. The carbon atom of the methoxyl group contributes with a hydrophobic interaction with Lysβ254.

Colchicine was re-docked in its binding pocket. The eptacyclic (tropolone) ring has a hydrophobic interaction with Alaα180. Trimethoxyphenyl moiety of colchicine is oriented towards the hydrophobic portion of the tubulin binding pocket. Metβ259, Asnβ258, Leuβ255, Lysβ254, Aspβ251, Alaβ250, Leuβ248, Leuβ242 and Cysβ241 are the representative aas of this portion of the pocket. Most of these aas also have hydrophobic interactions with compound **9b**, especially with the heterocyclic scaffold of the molecule, but also with the acrylonitrile linkage, as shown in Figure 1b. Figure 2 shows polar and hydrophobic interactions among compound **9b** and α- and β-tubulin subunits in the colchicine binding pocket. Methoxyl group is shown to be the most solvent-exposed portion of the molecule, pointing toward the outer portion of tubulin active site.

In the binding pocket, four aas (Serα178, Thrα179, Alaα180, Alaα181) were recognised to be crucial for the binding of colchicine. Using AutoDockTools, [27] last-mentioned four aas were set as flexible during the docking runs. Compound **A** best pose showed an affinity energy value of -6.7 kcal/mol, meanwhile, compound **9b** presented a ranked affinity energy of -7.4 kcal/mol. From these preliminary results of docking prediction, compound **9b**, and in general, the difluoro substitution on the main benzotriazole scaffold, could be considered beneficial for the affinity to the colchicine-binding site of tubulin. For this reason, the new series of (*E*)(*Z*)-2-(5,6-difluoro-(1*H*)2*H*-benzo[*d*][1,2,3]triazol-1(2)-yl)-3-(*R*)acrylonitrile derivatives was designed, synthesised and tested *in vitro* on different tumour cancer cells, as further reported in the present work.

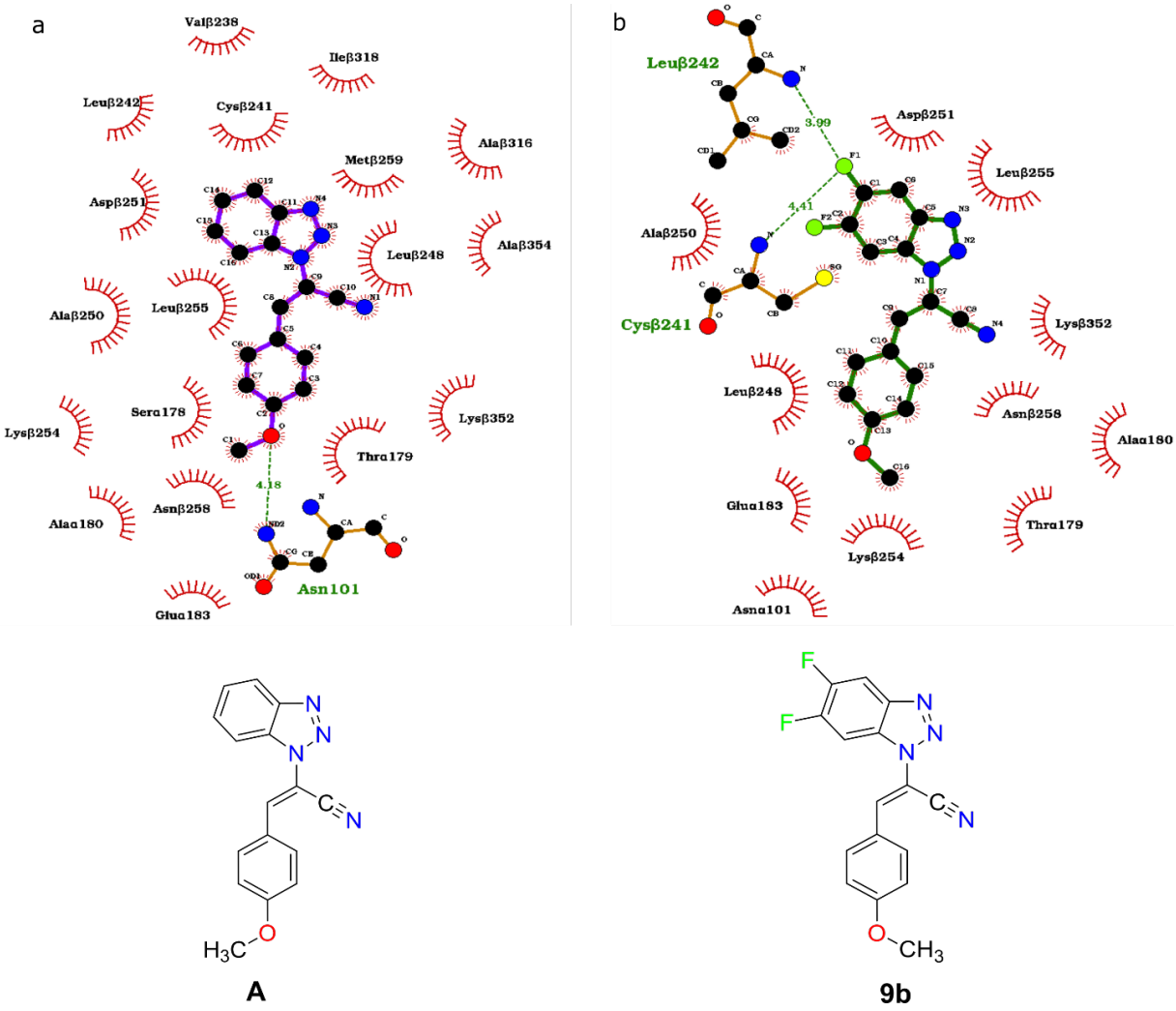

*Figure 1. Schematic comparison between the binding pose of compounds **A** (a) and **9b** (b) inside the tubulin binding pocket. H-bonds are depicted as green dashed lines and hydrophobic contacts as red hash marks. Atom colours: carbon, black; nitrogen, blue; fluorine, green; oxygen, red. Amino acids are labelled with the residue name, the chain and the correspondent number. The hashes in the ligand show atoms having hydrophobic interactions with aas. Distances are given in Å. Figure made by using LigPlot⁺.* [25]

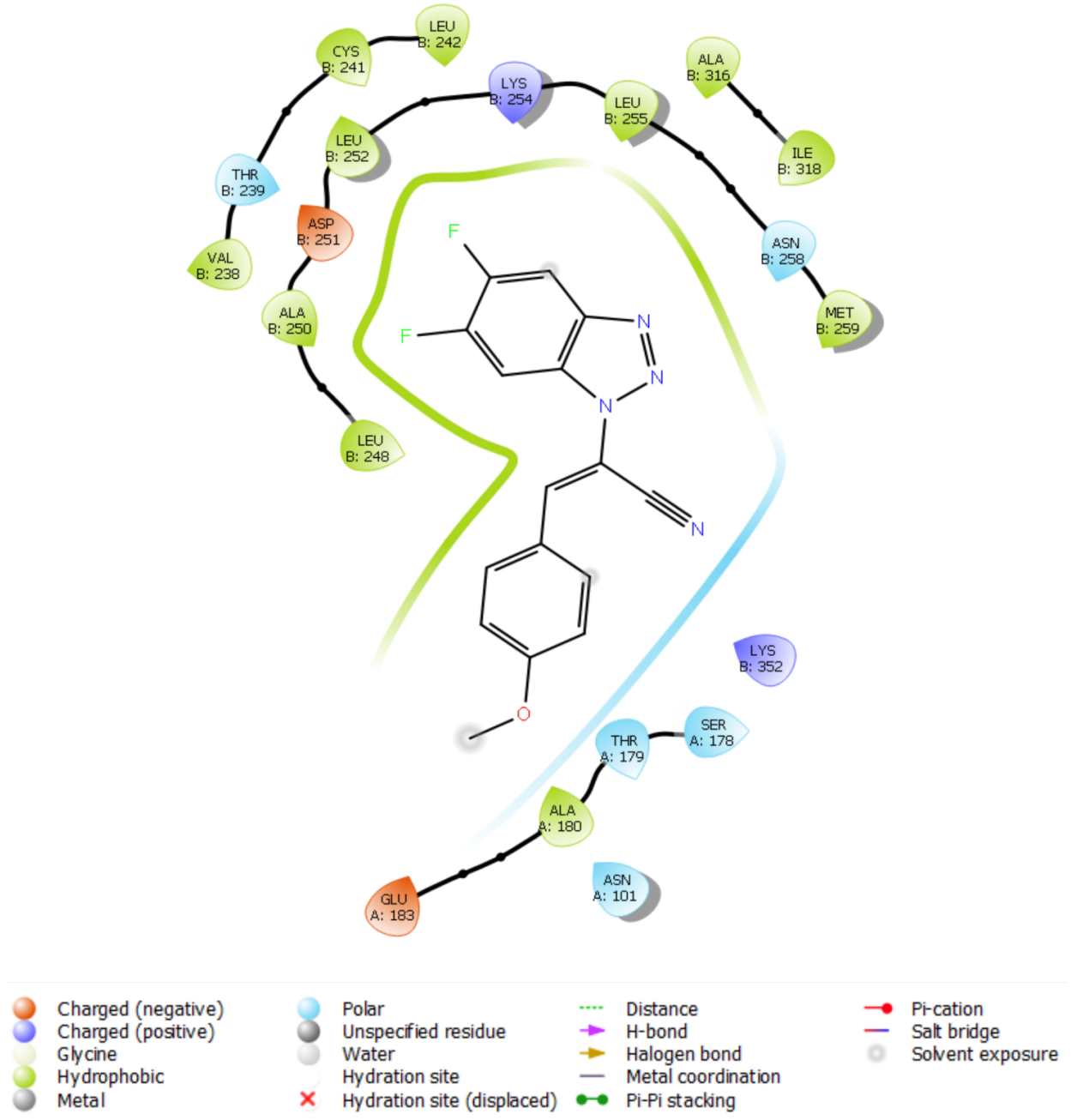

F*igure 2. Ligand Interaction Diagram and LID legend of the different interactions between compound* ***9b*** *and different amino acids in tubulin binding pocket. Residue markers are coloured according to residue type (green = hydrophobic, cyan = polar, red = negative, purple = positive). Green and cyan lines represent the interactions between* ***9b*** *and the different portions of the binding pocket. The gap in the line shows the opening of the pocket. Grey atom markers on the background of ligand structure represent the solvent-accessible surface area (SASA) of that atom, and the marker size represents the amount of exposure. Each protein residue is depicted as a "guitar peak": it points away from the ligand when the aa backbone faces towards the ligand, or it points to the ligand when the aa side chain faces towards the ligand. Cut-off default of 4 Å was used. Figure made by using Maestro.* [24]

2.2. Chemistry

The synthesis, as depicted in Scheme 1, starts with the commercially available 3,4-difluoroaniline (**1**), which was in first place acetylated, gaining compound **2**. The following nitration, hydrolysis and reduction bring to 4,5-difluorobenzene-1,2-diamine (**5**). The dianiline derivative **5** is cyclized with $NaNO_2$ in HCl, obtaining 5,6-difluorobenzotriazole (**6**). Reaction of **6** with chloroacetonitrile ($ClCH_2CN$) was performed, in the presence of KOH in acetonitrile, to obtain two geometric isomers bearing an acetonitrile chain on the triazole ring **7a**,**b** (Scheme 1).

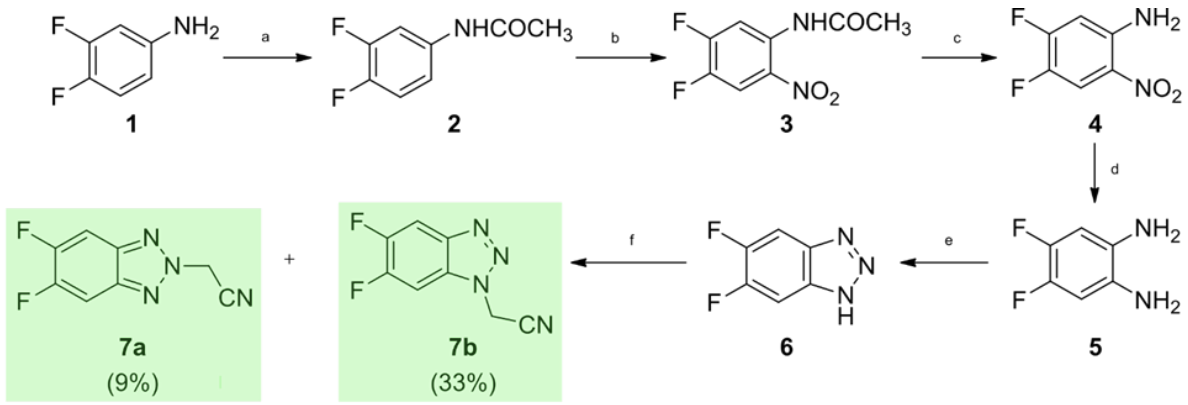

Reaction conditions: (a) $(CH_3COO)_2O$, 10 min, 0 °C; (b) KNO_3, H_2SO_4, 2h, r.t. ; (c) H_2SO_4 conc, 2h, reflux; (d) H_2, Pd/C, 2 h, r.t. ; (e) $NaNO_2$, HCl, 20 h, r.t. ; (f) $ClCH_2CN$, KOH, DMF, overnight, reflux.

*Scheme 1. Synthesis of intermediates 2-(5,6-difluoro-2H-benzo[d][1,2,3]triazol-2-yl)acetonitrile (7**a**) and 2-(5,6-difluoro-1H-benzo[d][1,2,3]triazol-1-yl)acetonitrile (7**b**).*

The final step (Scheme 2) comprises a Knoevenagel condensation between each acetonitrile isomer (**7a**,**b**) separately, and the appropriate, commercially purchased, aldehydes (**8a-j**), bringing to final (*E*)(*Z*)-2-(5,6-difluoro-(1*H*)2*H*-benzo[*d*][1,2,3]triazol-1(2)-yl)-3-(*R*)acrylonitrile derivatives **9a-j**, **10e**, and **11a**,**b**. The final step generally brings to the sole formation of the *E*-isomer. In some cases, the reaction generated a mixture where the *Z*-isomer has a very low yield, thus it is present in several NMR spectra, before the reaction work-up (as explained in Section 2.2.1 for compound **9i**), but then it could not be isolated in good yield to be fully characterised. Only in one case, a *Z*-isomer compound (**10e**) was purified from the reaction mixture and then characterised. The reaction was performed by one out of three different synthetic routes, (1) as previously described, [14–19] by using TEA (triethylamine) in toluene; (2) with DIMCARB (dimethylammonium dimethylcarbammate) used as base and reaction catalyst, in acetonitrile and (3) by using piperidine in acetonitrile, (Scheme 2). DIMCARB (in CH_3CN) also allowed to obtain compound **10e**, *p*-NO_2-derived *Z*-isomer, while using TEA (in toluene) as base gave the *E*-isomer **9e** as the major product of the Knoevenagel reaction. Compounds **13d**,**j** were obtained by Knoevenagel condensation between the 2-(1*H*-benzo[*d*][1,2,3]triazol-1-yl)acetonitrile isomer, synthesised as previously reported, [19] and the appropriate aldehydes **8d**,**j** (Scheme 2). The selection of substituents on the acrylonitrile moiety was based upon the best antimitotic activity properties of the series of compounds previously reported by us [14–19] or by colleagues. [28] As two new substituents were selected by the literature (4-hydroxyphenyl and isoquinolin-5-yl), we also designed new parental compounds of the lead **A**, thus

two new (*E*)-2-(1*H*-benzo[*d*][1,2,3]triazol-1-yl)-3-(*R*)acrylonitrile derivatives (**13d**,**j**) were synthesised.

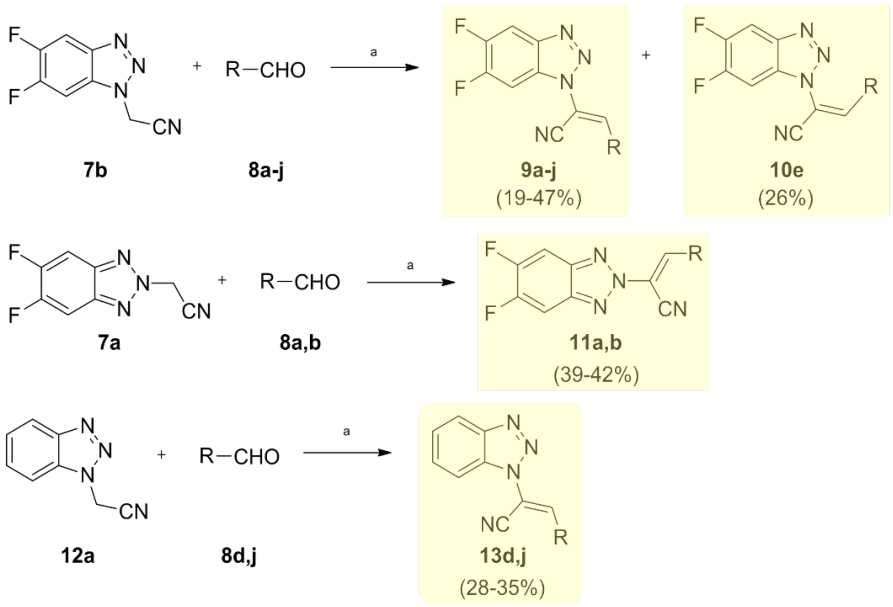

a: R = 4-CH_3-Ph; **b:** R = 4-OCH_3-Ph; **c:** R = 2,3,4-OCH_3-Ph; **d:** R = 4-OH-Ph; **e:** R = 4-NO_2-Ph; **f:** R = 4-F-Ph; **g:** R = 4-Cl-Ph; **h:** R = 4-Br-Ph; **i:** R = benzo[d][1,3]dioxol-5-yl; **j:** R = isoquinolin-5-yl.

*Scheme 2. Synthesis of (E)(Z)-2-(5,6-difluoro-(1H)2H-benzo[d][1,2,3]triazol-1(2)-yl)-3-(R)acrylonitrile (**9a-j**, **10e**, **11a,b**) and (E)-2-(1H-benzo[d][1,2,3]triazol-1-yl)-3-(R)acrylonitrile derivatives (**13d,j**).* [a]Reaction conditions: (1) TEA, toluene, 110 °C, or (2) DIMCARB, CH_3CN, 60 °C or (3) Piperidine, CH_3CN, 60 °C; properly chosen to get the full conversion.

2.2.1. *E*/*Z* isomers characterisation: one-dimensional NMR spectroscopy

Compound **9i** was chosen as the prototypical case for compounds reported in this manuscript since it was initially obtained as the mixture of both *E*- and *Z*-isomers (one was the major product, the other the minor one, not enough to be isolated and fully characterised). The ^{1}H-NMR spectrum clearly showed almost no superposition among the resonances due to the two different isomers together, with a relatively higher concentration of the *E*- one. This offered us the opportunity to investigate the two isomers more deeply and to fully characterise them in terms of chemical shift values. Resonance assignments for the compound **9i** (*E*-isomer) and the correspondent *Z*-isomer are shown in Figure 3.

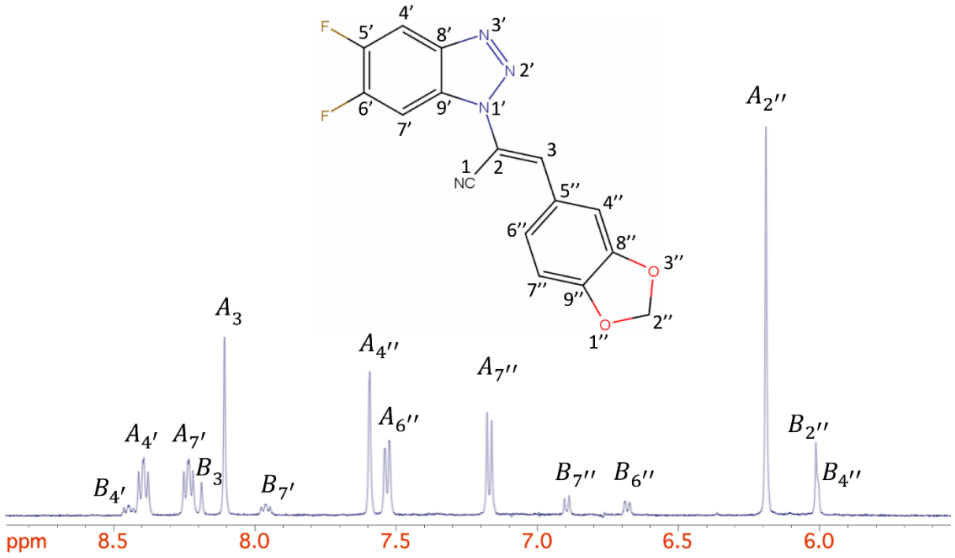

*Figure 3. [1]H-NMR spectrum and peaks assignment for compounds **9i** (E-isomer) peaks labelled with A and the correspondent Z-isomer, peaks labelled with B.*

As depicted in Figure 3, the presence of both the *E*- and the *Z*-isomers is revealed by two series of homologous resonances corresponding to two different concentrations (relative intensity). The resonances of the *E*-isomer are labelled with A, the *Z* one with B. Each resonance has been assigned according to the numbers beside the Lewis structure reported in the figure.
Each proton resonated at a significantly different chemical shift when the two isomers are compared. The highest shift is observed for protons 4", 6", 7" and 7', which are the ones closest to the unsaturation of the central acrylonitrile unit. Figure SI1 shows 1D-noesy spectra in order to better distinguish between *E* (**9a-j**, **11a,b** and **13d,j**) and *Z* (**10e**) isomers (detailed 1D-noesy characterisation in SI). Focusing on the vinylic CH, in the ^{1}H spectra there is a slight difference in chemical shift between the two isomers. On the contrary, in carbon spectra, there is a great displacement of the peak of the vinylic CH between *E*- and *Z*-isomer of the NO_2-derived compounds **9e** and **10e** (Figure SI2 in Supporting Information).

2.3. Biology

2.3.1. NCI60 in vitro screening

The ability to reduce the number of viable cells is one of the main features related to new anti-cancer drugs. The first *in vitro* anti-cancer screening was performed through the NCI60 test (NCI, Bethesda, USA). At the beginning, a single high dose of 10 µM of the compound was tested on the full NCI60 cell panel. The panel comprises a set of cancer lines from nine solid (non-small cell lung, colon, central nervous system - CNS, ovarian, renal, prostate and breast cancers) and haematological (leukaemia and melanoma) tumours. At 10 µM, 5',6'-difluoro-substituted 1*H*-benzotriazole derivatives (**9a-j**, **10e**) showed higher percentages of growth inhibition (GI) in comparison to 2*H*-benzotriazole derivatives (**11a,b**). All data from NCI60 are reported in Supporting Information (Figures SI6-25). At 10 µM, compound **9a** was selected as lead compound of this series showing the best scores and its antiproliferative activities on NCI60 cancer cells are reported in Figure 4.

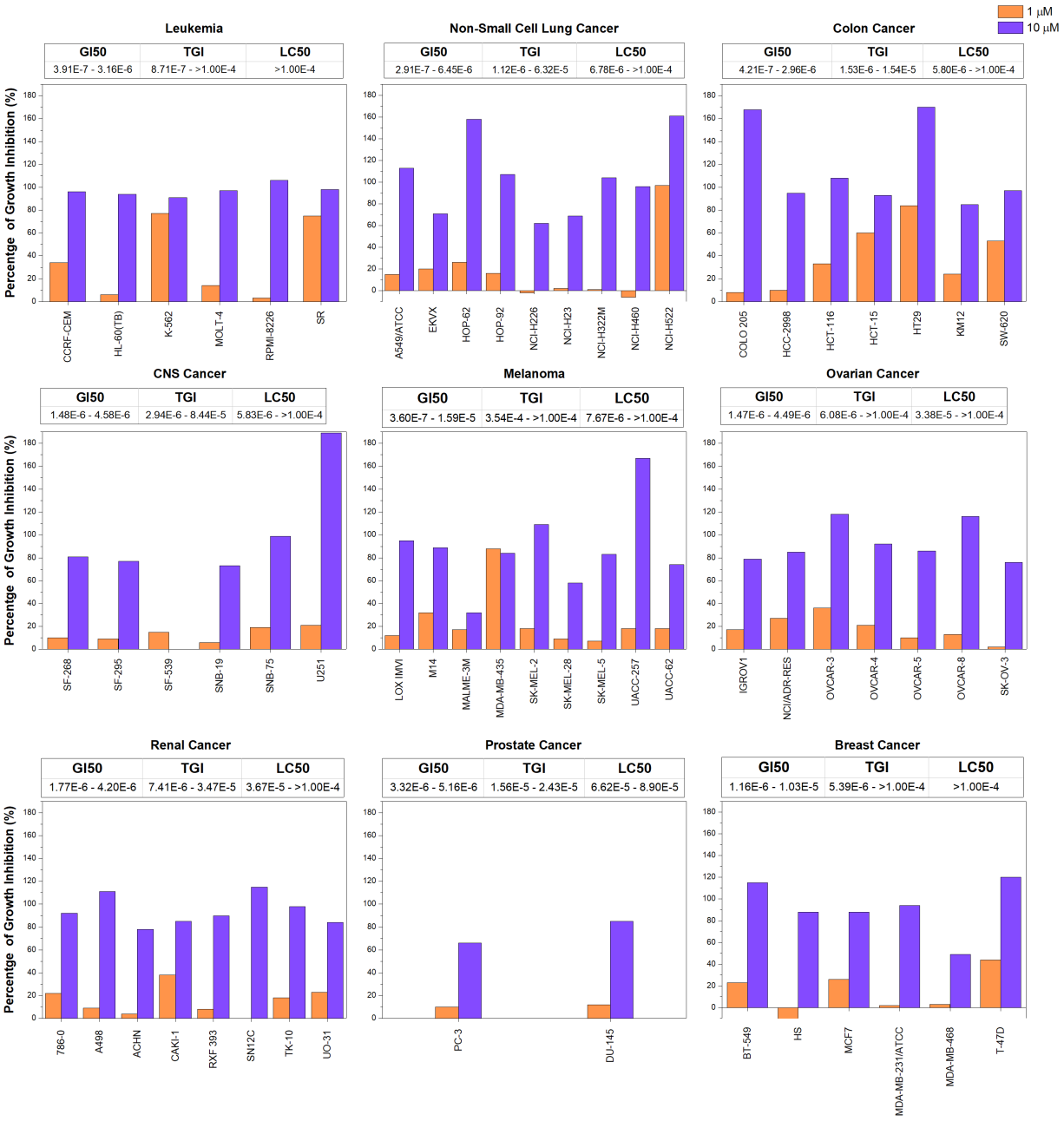

*Figure 4. Graphical illustration of antiproliferative activity for compound **9a** tested against NCI60 cell panel. Percentage of Growth Inhibition (%) is reported for each cell line tested, grouped for type of cancer. For each group, a range of GI_{50}, TGI and LC_{50} are reported; values are intended as µM.*

Compound **9a** showed GI percentages at about 100% against all leukaemia cell lines, and in general terms, it exhibits GI values around 60-100% against all the sixty solid and haematological cell lines (1% of growth against SNB-75 cell line of CNS cancer). In several instances, compound **9a** turned out cytotoxic against seventeen solid and haematological tumour cell lines with lethal percentages up to 90% (U251, CNS cancer cell line). Compounds **9a**, **9e**, **9g** and **9h** satisfied the pre-determined threshold inhibition criteria in a minimum number of cell lines and progressed to the second step of the 5-dose assay, from 100 µM to 10 nM. At 1 µM, compound **9a** presents GI percentages ranging

from 40 to 60% against eight tumour cell lines and 70-100% against further seven cell lines (93% against NCI-H522 cell line of Non-small cell lung cancer). General GI_{50} values are up to 0.1 μM, while LC_{50} and TGI values come up to 1 μM.

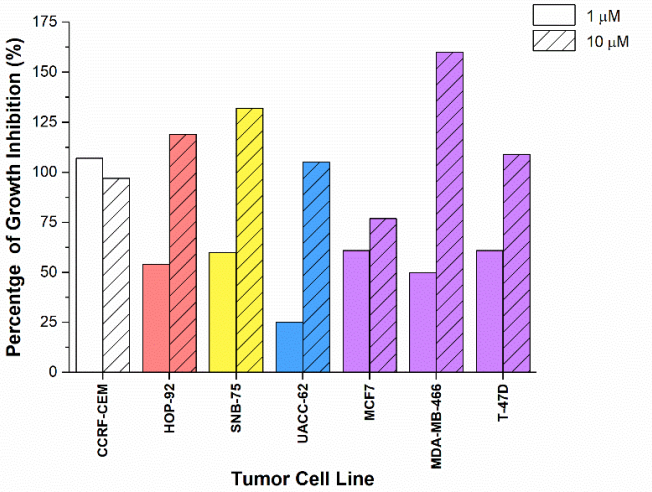

	GI50	TGI	LC50
Leukemia	2.53E-7 - 3.21E-6	2.43E-5 - >1.00E-4	>1.00E-4
NSC Lung Cancer	5.32E-7 - 2.32E-5	5.13E-6 - >1.00E-4	>1.00E-4
CNS Cancer	1.84E-7 - 3.24E-5	3.61E-6 - >1.00E-4	>1.00E-4
Melanoma	2.04E-6 - 7.71E-6	>1.00E-4	>1.00E-4
Breast Cancer	5.57E-7 - 2.97E-6	2.84E-6 - >1.00E-4	>1.00E-4

*Figure 5. Graphical illustration of representative antiproliferative activity results for compound **13j** tested against NCI60 cell panel. Seven cell lines were selected and reported coloured by type of cancer. The bar chart reports the percentage of Growth Inhibition for each cancer cell line when treated with **13j** at 1 or 10 μM concentration. The table shows a range of GI_{50}, TGI and LC_{50} values (μM) for each reported type of cancer.*

Regarding 1*H*-benzotriazole derivatives (**13d,j**), compound **13d** demonstrated a low GI rate, but, contrariwise, isoquinolin-5-yl derivative **13j** showed an interesting antiproliferative activity and was selected for the 5-doses dilution assay: at 10 μM the proliferation of the greatest part of tumour cell lines was inhibited with percentage values ranging between 70 and 100%, some of them were selected and reported in Figure 5. At 1 μM, it showed its best activity against CCRF-CEM leukaemia line, inhibiting completely the tumour cell growth. Compound **13j** also showed antiproliferative activity against six cell lines of four tumours (as depicted in Figure 5): it exhibited growth inhibition percentages of 50-60% against most of the reported cell lines at 1 μM.

*2.3.2. IC_{50} and Mechanism of action of **9a** against HeLa cells*

In order to understand if **9a** could be defined as a microtubule destabilising agent, as well as its previously reported parental compounds, [17,18] its antiproliferative activity was tested against HeLa cells. XTT was performed after 24 and 48 hours of treatment. Cells were treated at different concentrations of **9a** ranging between 0.1 and 5 μM, DMSO was used as control. Colorimetric assay

was carried out after 48 hours of treatment, the absorbance data were obtained and processed to calculate the percentage of cell viability. [29] A reduction of 50% of alive cells was detected after 48 hours of treatment with **9a** with an IC_{50} value of 3.2 µM.

To prove that **9a** was able to affect the HeLa cell cycle, flow cytometry was used to evaluate the changes in the DNA content after treatment. As shown in Figure 6, the administration of **9a** at 5 µM causes an increase of cells number in G2/M-phase (54%) compared to the control (30%) after 24 hours of treatment. This effect was even more evident at a higher concentration of 10 µM with a percentage of G2/M-phase cells of 66% after 24 hours. The increase of cells in G2/M-phase causes a contemporary decrease of G1-phase cells both at 5 µM (39%) and 10 µM (20%) compared to the control (65%). Results after 48 hours showed slight recovery of cells in G1-phase at 5 µM (41%) but a dramatic increase of cells in G2/M-phase (87%) proportional to the decrease of G1-phase rate (10%) after 48 hours of treatment at 10 µM.

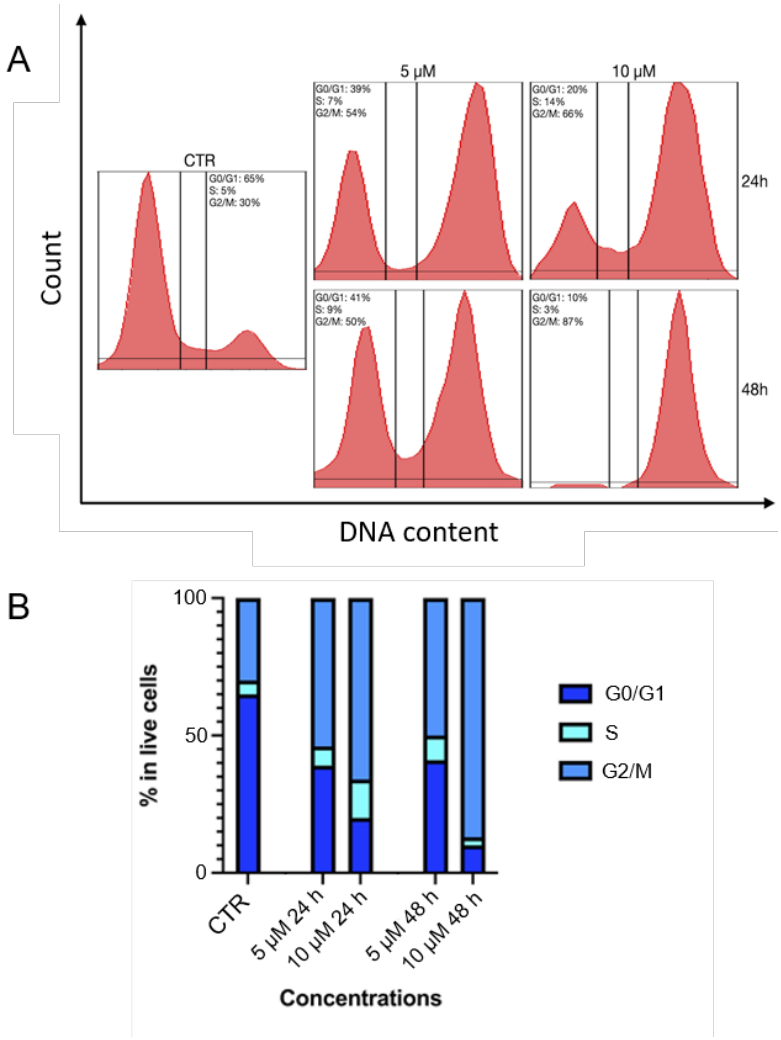

*Figure 6. Cell cycle phase distribution in HeLa cells after **9a** treatment. **A.** Representative cell cycle profiles of HeLa cells treated with 5 µM or 10 µM of **9a** for 24 or 48 h. Treatment with 5 µM of **9a** causes an accumulation of cells in G2/M phase after 24 hours with a completed block at 10 µM after 48 hours post-treatment. **B.** Percentages of cells in the different phases are shown.*

2.3.3. ***9a*** *slows the cytokinesis in HeLa cells*

With the aim to confirm the cell cycle impairment observed in Figure 6, we performed a fluorescence microscopy screening on HeLa cells treated with **9a** for 48 hours. Based on the previously described cell accumulation in G2/M phase we decided to count the number of incomplete cytokinesis events per field. As shown in Figure 7A-B, the amount of incomplete cell divisions increases starting from 0.3 µM compared to controls. We also observed an overall increase in cell dimension compared to controls (mock, untreated).

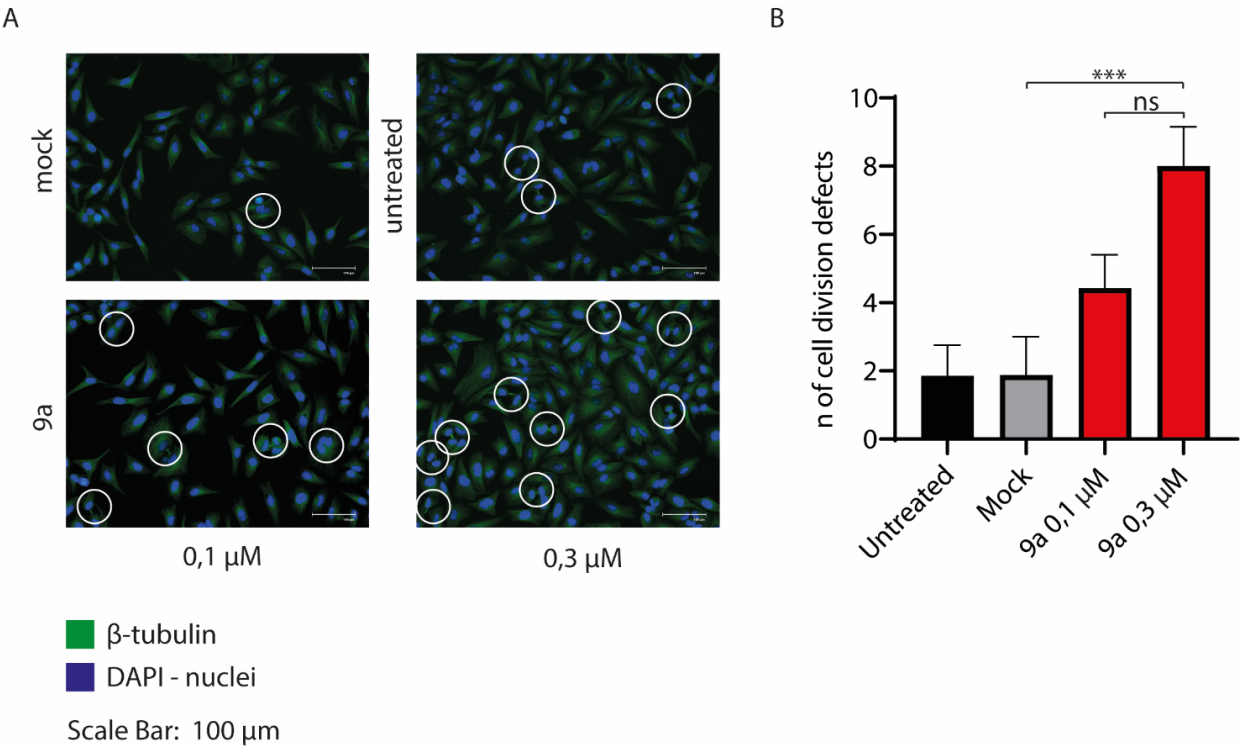

Figure 7. Fluorescence microscopy screening of cytokinesis. ***A.*** *Images taken 48 h treatment with* ***9a*** *and controls stained with β-tubulin, shows an increase of incomplete cell divisions starting at 0.3 µM.* ***B.*** *Kruskal-Wallis test with multiple comparisons performed on the number of incomplete cell division per field.* *** *P(*<0,0001); ns = not significant.

2.3.4. *Cytotoxicity evaluation of compound* ***9a*** *in presence or absence of efflux pump inhibitor (EPI)*

In order to test whether this chemical class of molecules could be client of extrusion pumps (EPs), often overexpressed in drug-resistant cancer cells, we tested the lead compound **9a** in cell-based association assay. Four cancer cell lines with EPs overexpression were selected. [30] Two kidney cancer (A498, A-704), one non-small cell lung cancer (A549) and one bladder cancer (HT1197) cell lines were selected for this experiment. Two of them, A498 and A549 cell lines were already used in the NCI screening and the results from the NCI60 cell line screening were used to select a concentration range of compound **9a** to be used in the association assay. The four cancer cell lines

were treated with the sole compound **9a** or in association with an extrusion pump inhibitor (EPI) from our group library, compound here labelled as **SS26**. The results are reported in Figure 8 and Figure SI21 and SI22. Figure 8 shows the Percentage of Growth (%) for each tumour cell line, at each time point at 5 different concentration of compound **9a** (1, 2, 4, 8 and 16 μM), alone and in association with our EPI at a fixed concentration (1 μM). The data are reported as Loess model with 95% confidence interval. The data collected at 24 hours time-point are presented for completeness but were not considered for the cytotoxic effect analysis since the cell growth is not yet stable at 24 hours after seeding. The results of the experiment at 48 and 72 hours clearly highlight that the association with EPI **SS26** resulted beneficial for the antiproliferative activity of **9a** against all the 4 tested tumour cell lines. The most striking results were obtained after 72 hours of treatment for all the tested cell lines. The cell growth inhibition was highly increased when **9a**+**SS26** were tested against A-704 cell line at both 48 and 72 hours. The most representative data concerned the two concentrations of 4 and 8 μM of compound **9a** since at 16 μM concentration the cells were saturated and the EPI effect was not detectable any longer. Figure SI21 presents the raw cell growth values, while Figure SI22 shows in bar charts the concentration-dependent efficacy.

We obtained two main pieces of information from this association assay, we proved that these small molecules are client of extrusion pumps with a negative effect on the antiproliferative activity. Furthermore, it is clearly shown that by increasing the concentration of derivative **9a** in the cytosol the antiproliferative activity is potentiated.

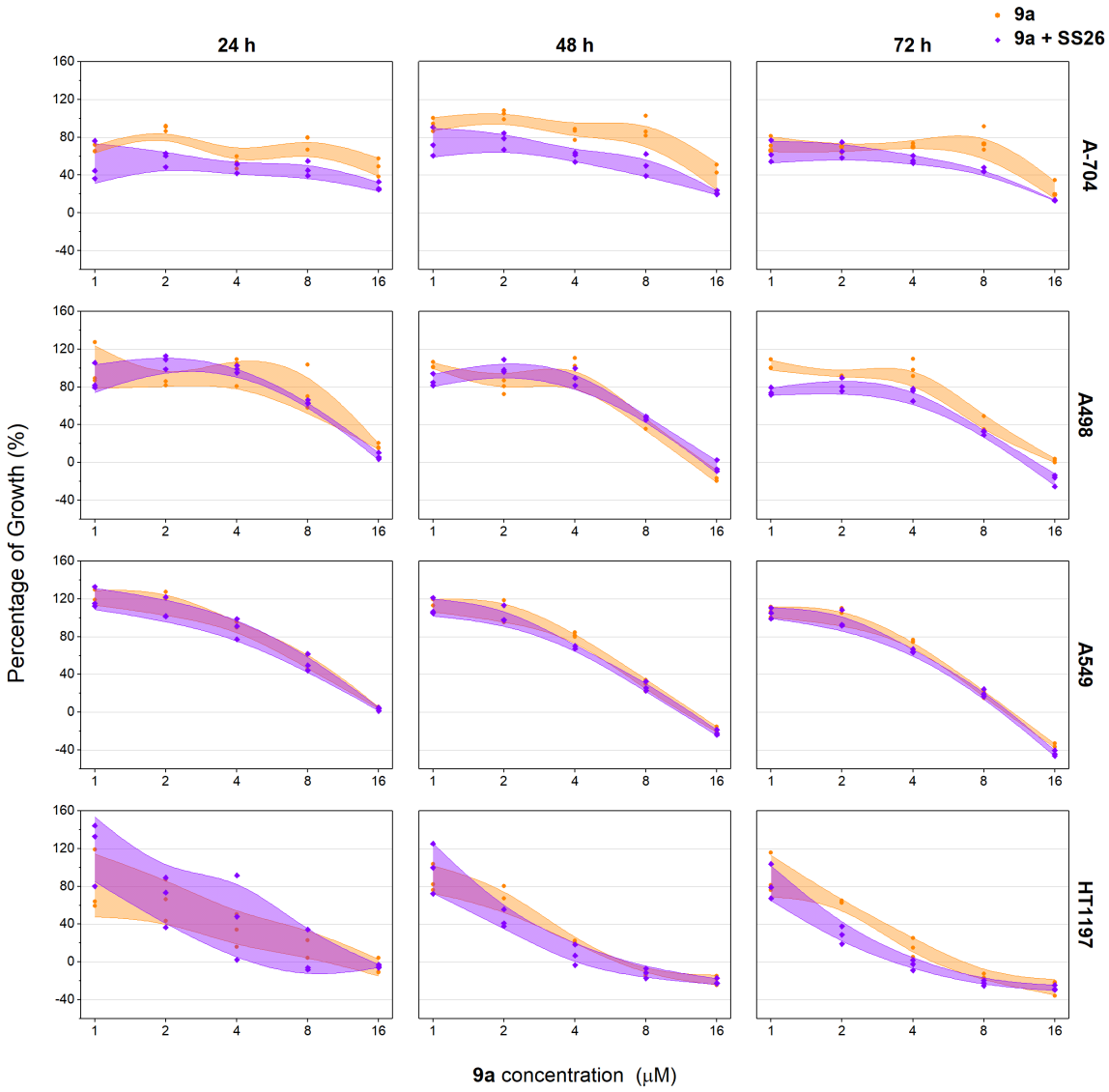

*Figure 8. Association assay. Percentage of Growth in cells treated with compound **9a** alone and in association with EPI **SS26**. Loess model, 95% Confidence interval.*

2.4. Physicochemical, pharmacokinetic and druglikeness predictions

SwissADME predictions (http://www.swissadme.ch) were employed to study different properties of this series of molecules. All the final derivatives **9a-j**, **11a-b** and **13d,j** were evaluated with these theoretic predictions. The results are summarised in Table 1 and the specific SwissADME outputs are reported in Figures SI28-41 in Supporting Information. According to the physicochemical properties, MWs (molecular weights) of the compounds are in a range of 262.27 and 372.33 g/mol. The rotatable bonds are between 2 and 5. H-bonds donor groups are in general 0 (only in few cases 1), while the number of H-bond acceptors is from 2 to 5. To complete the physicochemical characteristics, the TPSA (topological polar surface area) values were calculated from 54.50 and 100.32 Å^2. Regarding the lipophilicity/hydrophilicity properties, CLog $P_{o/w}$ takes values in the range

2.18 to 3.83, while Log *S* (one of the most common values to evaluate the water solubility of compounds) values are from -3.63 to -4.98. Most of the molecules are expected to be moderately water-soluble (one completely soluble, **13d**, and one poorly soluble, **9j**). All compounds are predicted to be able to be absorbed through the GI (gastrointestinal) membrane and to permeate the BBB (blood-brain barrier) membrane. While they are not theorised to be P-gp substrates, we demonstrated that compound **9a** is a P-gp substrate and as shown before, with the *in vitro* **9a**-EPI co-administration, the antiproliferative activity can increase if an EPI compound is present. All the compounds are drug-like molecules: they respect the Lipinski 'rule of five' with 0 violations and with a bioavailability score of 0.55 for all.

COMPOUND	Phisicochemical properties				Lipophilicity	Water Solubility		Pharmacokinetics			Druglikeness	
	Rotatable bonds	H-bond A	H-bond D	TPSA	CLog $P_{o/w}$	Log *S*	Solubility class	GI absorption	BBB permeant	P-gp substrate	Lipinski	BS
9a	2	5	0	54.50	3.53	-4.37	soluble (m)	High	Yes	No	Yes (0)	0.55
9b	3	6	0	63.73	3.19	-4.14	soluble (m)	High	No	No	Yes (0)	0.55
9c	5	8	0	82.19	3.18	-4.27	soluble (m)	High	No	No	Yes (0)	0.55
9d	2	6	1	74.73	2.79	-3.93	soluble (m)	High	Yes	No	Yes (0)	0.55
9e-10e	3	7	0	100.32	2.63	-4.12	soluble (m)	High	Yes	No	Yes (0)	0.55
9f	2	6	0	54.50	3.50	-4.23	soluble (m)	High	Yes	No	Yes (0)	0.55
9g	2	5	0	54.50	3.73	-4.67	soluble (m)	High	Yes	No	Yes (0)	0.55
9h	2	5	0	54.50	3.83	-4.98	soluble (m)	High	Yes	No	Yes (0)	0.55
9i	2	7	0	72.96	3.04	-4.17	soluble (m)	High	Yes	No	Yes (0)	0.55
9j	2	6	0	67.39	3.39	-4.55	soluble (p)	High	Yes	No	Yes (0)	0.55
11a	2	5	0	54.50	3.51	-4.73	soluble (m)	High	Yes	No	Yes (0)	0.55
11b	3	6	0	63.73	3.16	-4.49	soluble (m)	High	Yes	No	Yes (0)	0.55
13d	2	4	1	74.73	2.18	-3.63	soluble	High	Yes	No	Yes (0)	0.55
13j	2	4	0	67.39	2.79	-4.25	soluble (m)	High	Yes	No	Yes (0)	0.55

*Table 1. Physicochemical and pharmacokinetic properties, solubility and druglikeness of compounds **9a-j**, **10e**, **11a,b** and **13d,j**. In "physicochemical properties", A stands for acceptor and D for donors. TPSA represents the Topological Polar Surface Area, calculated in A^2. CLog $P_{o/w}$ is the Consensus Log P. Log S is a common unit for measuring the solubility, and it is calculated with the ESOL method. For the solubility, (m) stands for "moderately" and (p) for "poorly". GI means gastrointestinal, BBB blood-brain barrier. Druglikeness of the molecules are evaluated through the Lipinski 'rule of five' and (0) refers to the number of violations related to this rule. BS is the bioavailability score.*

3. Conclusions

In summary, we reported computational and experimental data which confirm that the newly synthesised series of 5',6'-difluorobenzotriazolacrilonitrile derivatives are considered as MDAs. We showed, through molecular docking studies, the different polar (fluorine bonds with cysteine and leucine residues, H-bonds, *e.g.* with different leucine residues) and nonpolar (with the hydrophobic portion of the pocket) interactions between **9b** and the tubulin binding site. This was also compared to the best-docked poses of colchicine and compound **A**. *E*,*Z*-designed derivatives (**9a-j**, **10e**, and **11a,b**, **13d,j**) were obtained through Knoevenagel condensation and fully characterised thanks to NMR spectroscopy experiments. The compounds were tested *in vitro* against the NCI60 cancer cell lines. We confirmed that the 1*H*-benzotriazole derivatives (**9a-j**, **10e**, **11a,b**) showed more activity than the 2*H*-benzotriazole derivatives (**11a,b**), and *p*-CH_3 derived compound **9a** was selected as lead compound of this library of molecules. At 1 μM concentration, it showed GI percentages between 40 and 60% against eight tumour cell lines and 70-100% against further seven cell lines. At the same

concentration, also compound **13j** exhibited growth inhibition percentage values of 50-60%. **9a** demonstrated its antiproliferative activity against HeLa cells with an IC_{50} = 3.2 μM, blocking most of the cells in G2/M phase and causing an increased number of cell division defects. Lead **9a** was also tested in co-administration with an extrusion pump inhibitor (SS26, 1 μM): the synergic activity of a microtubule destabilising agent and an EPI determined a more potent antiproliferative activity against four drug-resistant cancer cell lines. All designed and synthesised compounds showed good properties of predicted pharmacokinetics and druglikeness.

4. Material and Methods

4.1. Molecular Docking

AutoDock Vina 1.1.2. [31] version 1.5.6 was selected for its known sampling and scoring functions. [32] Tubulin-Colchicine complex (PDB code: 4O2B; resolution: 2.30 Å) structure was provided by the Protein Data Bank (rcsb.org). [33] Protein structures have been employed removing H_2O molecules, MES (buffer, 2-(*N*-morpholino)-ethanesulfonic acid), GOL (glycerol), ions (Ca^{2+}, Mg^{2+}), GTP (Guanosine-5'-triphosphate**)**, GDP (Guanosine-5'-diphosphate), but also chains C, D, E, F, in order to analyse the docking poses of ligands in a free binding pocket. The structures were visualised and analysed in PyMOL 2.3.4. AutoDockTools (ADT) [27] was used to obtain not only the PDBQT files of both protein structures and all ligands, but also to determine the docking Grid Box (30-30-30 Å for x,y,z coordinates). Docking was performed using the protein in its rigid form, or by making some amino acids flexible: Serα178, Thrα179, Alaα180, Alaα181. These amino acids are known to establish important H-bonds with the colchicine-binding pocket of tubulin. The exhaustiveness value was set to 8 and the number of poses to 10 for each Vina run. The binding energy range was imposed to be ≤ 2 kcal/mol above that of the best binding pose for each ligand. 2D-pictures of the binding interactions between ligands and the protein binding pocket were made with two molecular-graphics programs: LigPlot$^+$ v.2.2. and Maestro (Schrödinger package). LigPlot$^+$ processed in 2D-dimension the protein-ligand interaction with a cutoff of 5 Å from the centre of the ligand. Maestro's Ligand Interaction Diagram is a 2D binding site representation known for the accuracy in the placement of residues. The docking runs were conducted on a PC with an Intel® Core™ i7-9705H CPU @ 2.60 GHz with 8 GB RAM (operating system: Ubuntu 16.04, 6 CPUs for each run).

4.2. Chemistry

4.2.1. Synthetic Methods

The synthesis, as depicted in Scheme 1, starts with the commercially available 3,4-difluoroaniline (**1**), which was in the first place acetylated with acetic anhydride, gaining compound **2**. The following nitration of the amidic compound **2** with a solution of KNO_3 in H_2SO_{4conc} (concentrated H_2SO_4), resulted in the formation of nitro-derivative **3**. Then, 4,5-difluoro-2-nitroaniline **4** was obtained by hydrolytic deprotection with H_2SO_{4conc}. The reduction of nitro group brought to 4,5-difluorobenzene-1,2-diamine (**5**). The dianiline derivative **5** is cyclised with $NaNO_2$ in HCl, obtaining 5,6-difluorobenzotriazole (**6**). Reaction of **6** with chloroacetonitrile ($ClCH_2CN$) was performed, in the presence of KOH in acetonitrile, to obtain two geometric isomers bearing an acetonitrile chain on the triazole ring **7a**,**b** (Scheme 1). The final step (Scheme 2) corresponds to a Knoevenagel condensation between each acetonitrile isomer (**7a**,**b**), separately, and the appropriate, commercially purchased, aldehydes (**8a**-**j**), bringing to final (*E*)(*Z*)-2-(5,6-difluoro-(1*H*)2*H*-benzo[*d*][1,2,3]triazol-1(2)-yl)-3-(*R*)acrylonitrile derivatives **9a**-**j**, **10e**, and **11a**,**b**. The final step generally brings to the sole formation

of the *E*-isomer, only in one case a *Z*-isomer compound was identified and purified from the reaction mixture. A Knoevenagel condensation between 2-(1*H*-benzo[*d*][1,2,3]triazol-1-yl)acetonitrile **12a** and aldehydes **8d**,**j** (Scheme 2) gave final compounds **13d**,**j**. Compounds were purified by flash chromatography or by crystallisation from ethanol. For flash chromatography, Merck silica gel 60 was used with a particle size of 0.040-0.063mm (230-400 mesh ASTM), and a proper eluent mixture of petroleum spirit (PS), diethyl ether (DE), ethyl acetate (EA), chloroform ($CHCl_3$) and methanol (CH_3OH).

4.2.2. Chemical characterisation

Retention factors (R_f) were obtained using a mixture of petroleum spirit (PS) and ethyl acetate (EA) as eluents (8/2 respectively), to develop Thin Layer Chromatographies (TLCs), Merck F-254 plates were used. Melting points (m.p.) of the compounds were measured in a Köfler hot stage in open capillaries or Digital Electrothermal melting point apparatus and are uncorrected. The compounds were dissolved in CH_3CN for HPLC (concentration of 1.0-2.0 ppm) for ESI-MS characterisation. Mass spectra (full mass) were obtained on a Q Exactive Plus Hybrid Quadrupole-Orbitrap mass spectrometer of Thermo Fisher Scientific, in the positive-ion and negative-ion mode. The solutions were infused at a flow rate of 5.00 μL/min into the ESI chamber. The spectra were recorded in the *m/z* range 150–800 at a resolution of 140 000 and accumulated for at least 2 min in order to increase the signal-to-noise ratio. Measurements conditions for positive-ion were as follows: spray voltage 2300 V, capillary temperature 250 °C, sheath gas 10 (arbitrary units), auxiliary gas 3 (arbitrary units), sweep gas 0 (arbitrary units) and probe heater temperature 50 °C. Measurements conditions for negative-ion were as follows: spray voltage −1900 V, capillary temperature 250 °C, sheath gas 20 (arbitrary units), auxiliary gas 5 (arbitrary units), sweep gas 0 (arbitrary units), probe heater temperature 50 °C. ESI-MS spectra were analysed by using Thermo Xcalibur 3.0.63 software (Thermo Fisher Scientific), and the Xtract tool (integrated into the software) was used to extract the average deconvoluted monoisotopic masses. Nuclear Magnetic Resonance (NMR) spectra were registered in solutions in deuterated DMSO and recorded with a Bruker Avance III 400 NanoBay (400 MHz). ^{1}H-NMR chemical shifts are reported in parts per million (ppm) downfield from tetramethylsilane (TMS) used as internal standard. Chemical shift values are reported in ppm (δ) and coupling constants (J) are reported in Hertz (Hz). The assignment of exchangeable protons (OH and NH) was confirmed by the addition of D_2O. Signal multiplicities are represented as s (singlet), d (doublet), dd (doublet of doublets), ddd (doublet of doublets of doublets), t (triplet), m (multiplet) and wm (wide multiplet). ^{13}C-NMR chemical shifts are reported in downfield from tetramethylsilane (TMS) used as internal standard, jmod (*J*-modulated spin-echo for X-nuclei coupled to H-1 to determine number of attached protons) was selected as most suitable method. For the *E*/*Z*-isomers characterisation (Section 2.2.1.), ^{1}H-NMR spectra were acquired on an Agilent INOVA-500 spectrometer with an operative Larmor frequency of 500.3 MHz, by using a 6.1 μs pulse (90°), 1 s delay time, 1.5 s acquisition time, 8 transients and a spectral width of 9 kHz. ^{1}H-^{1}H correlation TOCSY experiments were recorded over the same spectral window using 2048 complex points and sampling each of the 256 increments with 8 scans and by applying 80 ms spin-lock with the MLEV-17 mixing scheme. The same acquisition parameters were applied for the acquisition of the NOESY experiments with 200 ms mixing time. In addition, a series of selective DPFGSE (Double Pulse Field Gradient Spin-Echo) one-dimensional NOESY [34] were performed with the same parameters as for standard ^{1}H acquisition with 128 transients and either 250, 500 and 750 ms mixing time. Resonance

assignments were obtained on the basis of relative intensity, chemical shift and fine structure, together with results from TOCSY and NOESY 2D spectra as well as the database at www.nmrdb.org. [35]

4.3. Biology

4.3.1. NCI60 testing screen: in vitro antiproliferative assay

The first *in vitro* anti-cancer screening was performed through the NCI60 test, provided by the Developmental Therapeutics Program of the National Cancer Institute (NCI, Bethesda, USA). At the beginning, a single high dose of 10 μM of the compound is tested in the full NCI60 cell panel. If the inhibition results agree with the selection criteria, the same compound can be tested again in 5x10-fold dilutions, from 100 μM up to 0.01 μM. More details about the NCI60 experiments are reported in the Supporting Information (Table SI1 and Figures SI6-25) and in the NCI website (https://dtp.cancer.gov).

4.3.2. HeLa cells culture

HeLa cells (human cervix epithelioid carcinoma) (ATCC, Rockville, MD) have been cultured with Dulbecco's Modified Eagle Medium (DMEM) (Gibco). Medium has been supplemented with 10% of Fetal Bovine Serum (FBS), 100 μg/mL streptomycin, 100 units/mL penicillin (Gibco) and 1% of l-glutamine. Cells were incubated at 37 °C in a humidified atmosphere containing 5% of CO_2.

4.3.3. Proliferation Assay on HeLa cells

HeLa cells were seeded at a density of 1500 cells/wells in a 96 wells-plate. After 24 hours from seeding, cells were treated with different concentrations of **9a** in a range between 0.1 μM and 5 μM for 24 and 48 hours in a final volume of 100 μL. Before using, **9a** has been resuspended in DMSO which has been used as control. After 24 and 48 hours of incubation with **9a**, XTT assay was performed using Cell Proliferation Kit II (Roche, Basel, Switzerland) and following the manufacture's protocol. Specifically, a volume of 100 μL with 74.5 μL of medium, 25 μL of labelling reagent and 0.5 μL of XTT electron coupling was added to each well and then incubated at 37 °C for 4 hours. After incubation, the absorbance was quantified at 490 nm using a spectrophotometric plate reader (SPECTRAMax 384 PLUS). Later on, data obtained were used for the calculation of IC_{50} value using Graphpad Prism software (San Diego, CA, USA). More than three independent experiments were carried out for each treatment and performed in triplicate.

4.3.4. Cell cycle analysis

Based on their phenotype and population doubling, HeLa cells were seeded at 50% of confluence on 6 cm dishes. After 24 hours, cells were treated with a concentration of 5 or 10 μM of **9a**. Later on, adherent and floating cells (dead cells) were initially centrifuged for 5 minutes at 3000 rpm, then washed in PBS and fixed with ice-cold ethanol at 70% in agitation on a vortex to dissolve cluster and permeabilise the membranes. After incubation overnight at -20 °C, fixed HeLa cells were washed twice with cold PBS and finally resuspended in 200 μL of a mix containing PBS and 20 μL/test of 7-AAD (Bioscience, San Diego, CA) and incubated at room temperature for 20 minutes. Flow cytometry was performed for cell cycle analysis using BD FACS CANTO II. For each sample 20000 events were collected and then analysed through BD FACS DIVA software.

4.3.5. Immunostaining

HeLa cells (10^5/well) were seeded 24 hours before treatment with **9a** (0.1 and 0.3 μM). After 48 hours cells were fixed with PFA (4%). Cells were permeabilised via three washes in PBS containing 0.3% Triton X-100 (PBST) and then blocked in PBST containing 1% BSA. Primary antibody β-tubulin (ab179512) was added in blocking solution for 2 hours. Then, 488 anti-rabbit secondary antibody (Alexa Fluor, Thermo Scientific) was incubated for 1 hour. Images were taken using 20x objectives (Evos FL2 Auto, Thermo Scientific). Statistical analysis was performed on 3 biological and technical replicates, using the Kruskal-Wallis test with multiple comparisons.

*4.3.6. Cytotoxicity evaluation of compound **9a** in presence or absence of efflux pump inhibitor (EPI)*

Cells were plated in a 384 multiwell plate and treated with **9a** (5 concentrations) in absence or presence (co-treatment) of EPI **SS26**. As negative control, cells were treated with vehicle solution (DMSO 0.3%). All treatments were performed at 0.3% DMSO concentration. Three technical replicates were performed. The number of alive and dead cells was quantified in each well of the multi-well plate immediately before compound addition and at 24, 48 and 72 hours of treatment by Kinetics of Cytotoxicity and Proliferation assay. Percentages of growth, percentages of dead cells, GI_{50}, TGI, and LC_{50} were calculated at each time point to evaluate reduction of proliferation and induction of cell death, data reported in Table SI2. *Cell culture.* A498, A-704, A549, and HT1197 cells were cultured in DMEM high glucose supplemented with 10% FBS, 2mM L-Glutamine, Non-essential aminoacids, 1mM Sodium Pyruvate, and Antibiotic Antimycotic Solution. Cells were cultured at 37 °C, 5% CO_2 humidified air. *Kinetics of Cell Proliferation and Cytotoxicity.* 24 hours before compound addition, 500 cells suspended in 20 μL phenol-red free complete medium containing SiR-DNA 0.5 μM (Tebu-bio SC007) and CellTox Green Dye 0.8x (Promega G8731) were plated in each well of a 384 Well Flat Clear Bottom Black Polystyrene TC-Treated Microplates (Corning 3764). The day after, 10 μL of serial dilutions of compounds in complete medium were added to each sample to obtain indicated treatment concentrations. Plating of cells, preparation of serial dilutions and addition of compounds to cells were performed using an automated liquid handling platform (Gilson Pipetmax). Immediately before compound addition to cells and after 24, 48 and 72 hours from treatment, images for far-red fluorescence (Cy5 filter), green fluorescence (GFP filter) and phase contrast were taken with objective 4x using automated digital widefield microscopy system BioTek Cytation 5. Cy5 filter: led cube 625nm, filter cube excitation 650 ± 30, emission 800 ± 90. GFP filter: led cube 465nm, filter cube excitation 469 ± 25, emission 525 ± 25. During each reading, cells were maintained at 37 °C, 5% CO_2. For each well, four images were taken and merged to cover the entire well. Number of nuclei stained by SiR-DNA in far-red fluorescence, and number of dead cells stained by CellTox Green Dye in green fluorescence, were automatically counted using BioTek Gen5 software. Alive cells were calculated by subtracting number of dead cells from total count of nuclei.

4.4. **Physicochemical, pharmacokinetic and druglikeness predictions**

SwissADME (http://www.swissadme.ch) predictions were performed for each final compound. The prediction does not discriminate between *E*- and *Z*-isomer. The physicochemical properties comprise typical molecular characteristics, including the TPSA (Topological Polar Surface Area). Log $P_{o/w}$ is calculated through different methods, and an average value is reported as consensus Log $P_{o/w}$. iLOGP, XLOGP3, WLOGP, MLOGP, SILICOS-IT methods contributed to the averaged Log *P*. The solubility and the Log *S* of each compound are also determined through several methods.

Pharmacokinetics properties are represented by the prediction of the GI (gastrointestinal), BBB (blood-brain barrier) and skin absorption, but also the affinity (substrate or inhibitor) for some important proteins (*e.g.* P-gp) and metabolic enzymes. Druglikeness is expressed through different methods, *e.g.* the Lipinski 'rule of five', [36] and the bioavailability score. Other druglikeness predictions were calculated with the Ghose, Veber, Egan and Muegge filters. Final considerations are the synthetic accessibility and the leadlikeness.

4.5 Experimental Section

4.6.1. Materials. 3,4-difluoroaniline (**1**) and the aldehydes (**8a–j**) were commercially available.

*4.5.1 N-(3,4-difluorophenyl)acetamide (**2**)*

Acetic anhydride (1 ml) was added dropwise to 3,4-difluoroaniline (**1**) (1 g, 0.8 ml, 7.8 mmol,) in an ice-bath (10 min). The white solid was filtrated, washed to reach neutral pH, then dried. $C_8H_7F_2NO$, MW: 171.14; 80% yield (1.1 g, 6.4 mmol), m.p. 107.3-109.4 °C; R_f 0.10. ^{1}H-NMR (DMSO-d_6): δ 10.16 (1H, s, NH), 7.77 (1H, ddd, $^1J_{H\text{-}F}$= 13.2 Hz, $^2J_{meta}$= 7.6 Hz, $^3J_{meta}$= 2.4 Hz, H-2), 7.36 (1H, dd, $^1J_{H\text{-}F}$= 19.3 Hz, $^2J_{meta}$= 9.2 Hz, H-5), 7.25 (1H, wm, H-6), 2.04 (3H, s, CH_3). ^{13}C-NMR (DMSO-d_6): δ 168.51 (C=O), 148.84 (C, dd, $^1J_{C\text{-}F}$= 242 Hz, $^2J_{C\text{-}F}$= 13 Hz, C-F), 144.99 (C, dd, $^1J_{C\text{-}F}$= 240 Hz, $^2J_{C\text{-}F}$= 13 Hz, C-F), 136.31 (C-N), 117.32 (CH), 115.11 (C, d, $J_{C\text{-}F}$= 8 Hz, CH-CF), 107.85 (C, d, $J_{C\text{-}F}$= 22 Hz, CH-CF), 23.86 (CH_3). ESI-MS (*m/z*): calcd for $C_8H_7F_2NO$ 172.05685, found 172.05676 $[M + H]^+$.

4.5.2 *N-(4,5-difluoro-2-nitrophenyl)acetamide (**3**)*

Compound **2** (1 g, 6.0 mmol) was dissolved in concentrated H_2SO_4 ($H_2SO_{4\ conc}$) in an ice-bath under magnetic stirring. A solution of KNO_3 (1.22 g, 12.0 mmol) in $H_2SO_{4\ conc}$ (3.26 ml) was added dropwise. The solution was brought to r.t. and stirred for 2 h. Next, the reaction was quenched with ice. The obtained precipitate was filtered off and washed with water to reach neutral pH. Pale-yellow solid; $C_8H_6F_2N_2O_3$, MW: 216.14; 79% yield (1 g, 4.6 mmol); m.p. 101.4-102.5 °C; R_f 0.60. ^{1}H-NMR (DMSO-d_6): δ 10.33 (1H, s, NH), 8.22 (1H, t, $^1J_{H\text{-}F}$= 8.8 Hz, H-5), 7.83 (1H, dd, $^1J_{H\text{-}F}$= 11.2 Hz, $^2J_{H\text{-}F}$= 7.6 Hz, H-2), 2.09 (3H, s, CH_3). ^{13}C-NMR (DMSO-d_6): δ 168.82 (C=O), 151.90 (C, dd, $^1J_{C\text{-}F}$= 253 Hz, $^2J_{C\text{-}F}$= 13 Hz, C-F), 145.04 (C, dd, $^1J_{C\text{-}F}$= 246 Hz, $^2J_{C\text{-}F}$= 14 Hz, C-F), 137.45 (C-N), 129.55 (CH), 114.89 (C, d, $J_{C\text{-}F}$= 10 Hz, CH-CF), 113.43 (C, d, $J_{C\text{-}F}$= 22 Hz, CH-CF), 23.39 (CH_3). ESI-MS *m/z* calcd for $C_8H_6F_2N_2O_3$ 217.10478, found 217.04193 $[M + H]^+$.

4.5.3 *4,5-difluoro-2-nitroaniline (**4**)*

Intermediate **3** (1 g, 4.6 mmol) was dissolved in $H_2SO_{4\ conc}$ (10 ml) under reflux (2 h). Next, the reaction was quenched with ice. A precipitate was obtained, then filtered off and washed with water to reach pH. Yellow solid; $C_6H_4F_2N_2O_2$, MW: 174.11; 61% yield (1.0 g, 5.7 mmol); m.p. 95.6-105.5 °C; R_f 0.53. ^{1}H-NMR (DMSO-d_6): δ 7.99 (1H, dd, $^1J_{H\text{-}F}$= 11.0 Hz, $^2J_{H\text{-}F}$= 8.4 Hz, H-5), 7.56 (2H, s, NH_2), 6.96 (1H, dd, $^1J_{H\text{-}F}$= 12.8 Hz, $^2J_{H\text{-}F}$= 7.2 Hz, H-2). ^{13}C-NMR (DMSO-d_6): δ 154.67 (C, dd, $^1J_{C\text{-}F}$= 126 Hz, $^2J_{C\text{-}F}$= 15 Hz, C-F), 144.63 (C, d, $J_{C\text{-}F}$= 12 Hz, C), 139.89 (C-F), 125.06 (C-NH_2), 110.93 (CH-CF), 105.41 (C, d, $J_{C\text{-}F}$= 21 Hz, CH-CF). ESI-MS *m/z* calcd for $C_6H_4F_2N_2O_2$ 175.03136, found 174.95352 $[M + H]^+$.

4.5.4 *4,5-difluorobenzene-1,2-diamine (**5**)*

Compound **4** (2 g, 11.5 mol) was dissolved in ethanol (200 ml). Pd/C (0.20 g, 10 % w/w) was added. The hydrogenation was performed with the shaking hydrogenation reactor (open tank, 1.5 h). The

Pd/C was filtered off and the solution was concentrated in vacuo to obtain a brown oil, which was purified via flash chromatography with DE; Brown solid; $C_6H_6F_2N_2$, MW: 144.12; 98% yield (1.62 g, 11.2 mmol); m.p. 111.6-117.2 °C; R_f 0.10. ^{1}H-NMR (DMSO-d_6): δ 7.04 (2H, t, $^1J_{H-F}$= 10.4 Hz, H-2,5), 5.33 (4H, s, 2NH_2). ^{13}C-NMR (DMSO-d_6): δ 141.14 (2C, dd, $^1J_{C-F}$= 231 Hz, $^2J_{C-F}$= 15Hz, C-F), 131.46 (2C-NH_2), 102.34-101.71 (2C, m, CH-F). ESI-MS *m/z* calcd for $C_6H_6F_2N_2$ 145.05718, found 145.05730 $[M + H]^+$.

4.5.5 *5,6-difluoro-1H-benzo[d][1,2,3]triazole (**6**)*

Compound **5** (1.65 g, 11.0 mmol) was dissolved in HCl 2 N (114 ml) in an ice-bath. An aqueous solution of $NaNO_2$ (1.63 g, 0.3 mol) was added dropwise. The solution was brought to r.t., then extracted with DE. Yellow solid; $C_6H_3F_2N_3$, MW: 155.11; 43% yield (0.8 g, 5.0 mmol); m.p. 179-181 °C; R_f 0.16. Spectra correspondent to lit. [37] δ ESI-MS *m/z* calcd for $C_6H_4F_2N_4$ 154.02113, found 154.02127 $[M - H]^-$.

4.5.6 *Synthesis and characterisation of the intermediates 2-(5,6-difluoro-1H-benzo[d][1,2,3]triazol-1-yl)acetonitrile (**7a**) and 2-(5,6-difluoro-1H-benzo[d][1,2,3]triazol-1-yl)acetonitrile (**7b**)*

Compound (**6**) (2.4 g, 15.3 mmol), KOH (0.95 g, 16.9 mmol) and chloroacetonitrile (0.9 ml, 1.0 g, 13.8 mmol) were dissolved in acetonitrile (20 ml), at 80 °C under reflux overnight. The solution was concentrated in vacuo and purified via flash chromatography (PS/EA 8/2). These reaction conditions have a good influence on the selective formation of the 1-isomer compared to the 2-isomer (ratio 3:1). (**7a**) Orange solid; $C_8H_4F_2N_4$, MW: 194.14; 9% yield (0.26 g, 1.3 mmol); m.p. 97.3-99.1 °C; R_f 0.20. ^{1}H-NMR (DMSO-d_6): δ 8.17 (2H, t, $^1J_{H-F}$= 8.8 Hz, H-4,7), 6.28 (2H, s, CH_2). ^{13}C-NMR (DMSO-d_6): δ 150.85 (2C, d, $^1J_{C-F}$= 249.2 Hz, $^2J_{C-F}$= 19.3 Hz, C-F), 140.13 (2C, t, $^1J_{C-F}$= 6.0 Hz, C=N), 114.12 (C≡N), 104.30 (2C, m, CH-CF), 44.0 (CH_2). ESI-MS *m/z* calcd for $C_8H_4F_2N_4$ 193.03203, found 193.03246 $[M - H]^-$. (**7b)** Yellow solid; $C_8H_4F_2N_4$, MW: 194.14; 33% yield (0.98 g, 5.0 mmol); m.p. 129.2-131.3 °C; R_f 0.18 (PS/EA 7/3). ^{1}H-NMR (DMSO-d_6): δ 8.29 (1H, dd, $^1J_{H-F}$= 10.0 Hz, $^2J_{H-F}$= 7.2 Hz, H-4), 8.21 (1H, dd, $^1J_{H-F}$= 9.6 Hz, $^2J_{H-F}$= 6.8 Hz, H-7), 6.14 (2H, s, CH_2). ^{13}C-NMR (DMSO-d_6): δ 150.87 (1C, dd, $^1J_{C-F}$= 240.6 Hz, $^2J_{C-F}$= 16.8 Hz, C-F), 148.41 (1C, dd, $^1J_{C-F}$= 233.5 Hz, $^2J_{C-F}$= 22.0 Hz, C-F), 140.32 (1C, d, $^1J_{C-F}$= 11.0 Hz, C=N), 128.79 (1C, d, $^1J_{C-F}$= 12.0 Hz, C=N), 114.76 (C≡N), 106.65 (1C, dd, $^1J_{C-F}$= 20.4 Hz, CH), 98.53 (1C, d, $^1J_{C-F}$= 25.0 Hz, CH), 36.01 (CH_2). ESI-MS *m/z* calcd for $C_6H_4F_2N_4$ 193.03203, found 193.03242 $[M - H]^-$.

*4.6.7. General procedure for final compounds **9a-j**, **10e**, **11a,b** and **13d,j**.* Compounds **9a-j** and **10e** were obtained from **7b** and **8a-j** (ratio 1:1), **11a,b** from **7a** and **8a,b** (ratio 1:1) and **13d,j** from **12a** and **8d,j** (ratio 1:1). Triethylamine (TEA, ratio 1:1+20%) was used as a base for products **9a-c,e-j**, **10e** and **11a,b**, in toluene as a solvent at 110 °C. DIMCARB (ratio 1:1+20%) was used as a catalyst for products **9d** and **13d**, in acetonitrile at 60 °C. Piperidine was used as a base for product **13j**, in acetonitrile at 60 °C. Some of the final compounds were (1) filtrated and crystallised from EtOH, (2) some were worked-up through liquid chromatography.

4.5.7 *(E)-2-(5,6-difluoro-1H-benzo[d][1,2,3]triazol-1-yl)-3-(p-tolyl)acrylonitrile (**9a**)*

Work-up procedure (2): PS/EA 9.5/0.5. White solid; $C_{16}H_{10}F_2N_4$, MW: 296,28; 45% yield (0.24 g, 0.8 mmol); m.p. 121.4-122.5 °C; R_f 0.72. ^{1}H-NMR (DMSO-d_6): δ 8.50 (1H, dd, $^1J_{H-F}$= 10.0 Hz, $^2J_{H-F}$= 7.2 Hz, H-4'), 8.38 (1H, dd, $^1J_{H-F}$= 9.8 Hz, $^2J_{H-F}$= 7.2 Hz, H-7'), 8.28 (1H, s, =CH), 7.98 (2H, d,

$^{1}J_{H\text{-}H}$ = 8.0 Hz, H-2",6"), 7.51 (2H, d, $^{1}J_{H\text{-}H}$ = 8.4 Hz, H-3",5"), 2.48 (3H, s, CH_3). ^{13}C-NMR (DMSO-d_6): δ 151.34 (1C, dd, $^{1}J_{H\text{-}F}$= 241.2 Hz, $^{2}J_{H\text{-}F}$= 16.6 Hz, C-F), 148.63 (1C, dd, $^{1}J_{H\text{-}F}$= 244.5 Hz, $^{2}J_{H\text{-}F}$= 16.2 Hz, C-F), 142.61 (C-CH_3), 142.43 (=CH), 140.6 (1C, d, $J_{H\text{-}F}$= 10.4 Hz, C=N), 129.80 (4C, m, CH), 128.08 (1C, d, $J_{H\text{-}F}$= 12.0 Hz, C=N), 127.68 (C), 114.15 (C≡N), 107.04 (1C, d, $^{1}J_{C\text{-}F}$= 20.8 Hz, CH-CF), 104.71 (C=CH), 99.65 (1C, d, $^{1}J_{C\text{-}F}$= 24.6 Hz, CH-CF), 21.13 (CH_3). ESI-MS *m/z* calcd for $C_{16}H_{10}F_2N_4$ 297.09463, 298.09798, found 297.09467, 298.09808 $[M + H]^+$.

4.5.8 *(E)-2-(5,6-difluoro-1H-benzo[d][1,2,3]triazol-1-yl)-3-(4-methoxyphenyl)acrylonitrile (**9b**)*
Work-up procedure (1). Brown solid; $C_{16}H_{10}F_2N_4O$, MW: 312,28; 37% yield (0.18 g; 0.6 mmol); m.p. 102.8-103.4 °C; R_f 0.48. ^{1}H-NMR (DMSO-d_6): δ 8.43 (1H, dd, $^{1}J_{H\text{-}F}$= 9.8 Hz, $^{2}J_{H\text{-}F}$= 7.2 Hz, H-4'), 8.29 (1H, dd, $^{1}J_{H\text{-}F}$= 9.4 Hz, $^{2}J_{H\text{-}F}$= 7.2 Hz, H-7'), 8.18 (1H, s, =CH), 8.02 (2H, d, $J_{H\text{-}H}$= 8.8 Hz, H-2",6"), 7.21 (2H, d, $J_{H\text{-}H}$= 8.8 Hz, H-3",5"), 3.89 (3H, s, OCH_3). ^{13}C-NMR (DMSO-d_6): δ 162.42 (C-OCH_3), 151.30 (1C, dd, $^{1}J_{H\text{-}F}$= 250.0 Hz, $^{2}J_{H\text{-}F}$= 16.7 Hz, C-F), 148.62 (1C, dd, $^{1}J_{H\text{-}F}$= 244.0 Hz, $^{2}J_{H\text{-}F}$= 16.3 Hz, C-F), 142.79 (=CH), 140.52 (1C, d, $J_{H\text{-}F}$= 10.4 Hz, C=N), 131.97 (2CH), 128.20 (1C, d, $J_{H\text{-}F}$= 12.3 Hz, C=N), 122.71 (C), 114.85 (2CH), 114.57 (C≡N), 106.99 (1C, d, $^{1}J_{C\text{-}F}$= 20.9 Hz, CH-CF), 102.57 (C=CH), 99.52 (1C, d, $^{1}J_{C\text{-}F}$= 24.6 Hz, CH-CF), 55.58 (CH_3). ESI-MS *m/z* calcd for $C_{16}H_{10}F_2N_4O$ 313.08954, 314.09290, found 313.08945, 314.09280 $[M + H]^+$.

*4.5.9 (E)-2-(5,6-difluoro-1H-benzo[d][1,2,3]triazol-1-yl)-3-(2,3,4-trimethoxyphenyl)acrylonitrile (**9c**)*
Work-up procedure (2): PS/EA 9/1. Yellow solid; $C_{18}H_{14}F_2N_4O_3$, MW: 344,32; 21% yield (0.1 g, 0.3 mmol); m.p. 119.3-120.6 °C; R_f 0.43. ^{1}H-NMR (DMSO-d_6): δ 8.44 (1H, dd, $^{1}J_{H\text{-}F}$= 9.6 Hz, $^{2}J_{H\text{-}F}$= 7.2 Hz, H-4'), 8.21 (1H, dd, $^{1}J_{H\text{-}F}$= 9.6 Hz, $^{2}J_{H\text{-}F}$= 6.8 Hz, H-7'), 8.11 (1H, s, C=CH), 7.94 (1H, d, $J_{H\text{-}H}$= 8.8 Hz, H-6"), 7.13 (1H, d, $J_{H\text{-}H}$= 8.8 Hz, H-5"), 3.94 (3H, s, OCH_3), 3.90 (3H, s, OCH_3), 3.81 (3H, s, OCH_3). ^{13}C-NMR (DMSO-d_6): δ 151.17 (C-OCH_3), 153.16 (2C-OCH_3), 141.54 (C), 140.32 (CF), 138.04 (CH), 128.44 (CF), 123.56 (CH), 116.76 (2C), 114.30 (C≡N), 108.47 (CH), 107.06 (1C, d, $^{1}J_{C\text{-}F}$= 21.6 Hz, CH-CF), 104.09 (C=CH), 99.20 (1C, d, $^{1}J_{C\text{-}F}$= 24.7 Hz, CH-CF), 61.82 (OCH_3), 60.43 (OCH_3), 56.19 (OCH_3). ESI-MS *m/z* calcd for $C_{18}H_{14}F_2N_4O_3$ 373.11067, 374.11403, found 373.11124, 374.11432 $[M + H]^+$; calcd 395.092962, 396.09597, found 395.09296, 396.09625 $[M + Na]^+$; calcd 411.06656, found 411.06683 $[M + K]^+$.

*4.5.10 (E)-2-(5,6-difluoro-1H-benzo[d][1,2,3]triazol-1-yl)-3-(4-hydroxyphenyl)acrylonitrile (**9d**)*
Work-up procedure (1). Yellow solid; $C_{15}H_8F_2N_5O$, MW: 298.25; 29% yield (0.12 g, 0.40 mmol); m.p. 178.4-180,6 °C; R_f 0.18. ^{1}H-NMR (DMSO-d_6): δ 10.59 (1H, s, OH), 8.41 (1H, dd, $^{1}J_{H\text{-}F}$= 9.6 Hz, $^{2}J_{H\text{-}F}$= 7.2 Hz, H-4'), 8.25 (1H, dd, $^{1}J_{H\text{-}F}$= 9.0 Hz, $^{2}J_{H\text{-}F}$= 6.8 Hz, H-7'), 8.09 (1H, s, =CH), 7.92 (2H, d, $J_{H\text{-}H}$= 8.0 Hz, H-2",6"), 7.0 (2H, d, $J_{H\text{-}H}$= 8.0 Hz, H-3",5"). ^{13}C-NMR (DMSO-d_6): δ 161.54 (C-OH), 151.28 (1C, dd, $^{1}J_{H\text{-}F}$= 249.0 Hz, $^{2}J_{H\text{-}F}$= 17.0 Hz, C-F), 148.59 (1C, dd, $^{1}J_{H\text{-}F}$= 244.5 Hz, $^{2}J_{H\text{-}F}$= 17.0 Hz, C-F), 143.62 (CH=C), 140.46 (1C, d, $J_{H\text{-}F}$= 10.0 Hz, C=N), 132.31 (2CH), 128.30 (1C, d, $J_{H\text{-}F}$= 12.0 Hz, C=N), 121.11 (C), 116.23 (2CH), 114.81 (C≡N), 106.94 (1C, d, $^{1}J_{C\text{-}F}$= 21.0 Hz, CH-CF), 101.17 (C=C), 99.39 (1C, d, $^{1}J_{C\text{-}F}$= 25.0 Hz, CH-CF). ESI-MS *m/z* calcd for $C_{15}H_8F_2N_5O$ 297.05824, 298.06160, 299.06495, found 297.05939, 298.06268, 299.06622 $[M - H]^-$.

*4.5.11 (E)-2-(5,6-difluoro-1H-benzo[d][1,2,3]triazol-1-yl)-3-(4-nitrophenyl)acrylonitrile (**9e**)*
Work-up procedure (2): PS/EA 8/2. Yellow powder; $C_{15}H_7F_2N_5O_2$, MW: 327.25; 24% yield (0.11 g, 0.3 mmol); m.p. 151.1-152.6 °C; R_f 0.46. ^{1}H-NMR (DMSO-d_6): δ 8.51-8.42 (2H, m, H-4',7'), 8.48

(2H, d, J_{H-H}= 8.8 Hz, H-3",5"), 8.43 (1H, s, =CH), 8.23 (2H, d, J_{H-H}= 8.4 Hz, H-2",6"). ^{13}C-NMR (DMSO-*d*$_6$): δ 151.47 (1C, dd, $^1J_{H-F}$= 249.5 Hz, $^2J_{H-F}$= 17.0 Hz, C-F), 148.70 (1C, dd, $^1J_{H-F}$= 245.0 Hz, $^2J_{H-F}$= 16.0 Hz, C-F), 148.48 (C-NO_2), 140.84 (1C, d, J_{H-F}= 10.0 Hz, C=N), 137.61 (=CH), 137.03 (C), 130.79 (2CH), 127.71 (1C, d, J_{H-F}= 12.0 Hz, C=N), 124.13 (2CH), 113.15 (C≡N), 109.56 (C=CH), 107.23 (1C, d, $^1J_{C-F}$= 20.0 Hz, CH-CF), 100.17 (1C, d, $^1J_{C-F}$= 24.0 Hz, CH-CF). ESI-MS *m/z* calcd for $C_{15}H_7F_2N_5O_2$ 328.06406, found 328.06406 $[M + H]^+$.

*4.5.12 (E)-2-(5,6-difluoro-1H-benzo[d][1,2,3]triazol-1-yl)-3-(4-fluorophenyl)acrylonitrile (**9f**)*
Work-up procedure (1). Light brown solid; $C_{15}H_7F_3N_4$, MW: 300,24; 19% yield (0.06 g, 0.2 mmol); m.p. 135.3-136.4 °C; R_f 0.67. ^{1}H-NMR (DMSO-*d*$_6$): δ 8.46 (1H, dd, $^1J_{H-F}$= 9.8 Hz, $^2J_{H-F}$= 7.2 Hz, H-4'), 8.35 (1H, dd, $^1J_{H-F}$= 10.0 Hz, $^2J_{H-F}$= 6.8 Hz, H-7'), 8.28 (1H, s, =CH), 8.10 (2H, dd, J_{H-H}= 8.4 Hz e J_{H-H}= 5.2 Hz, H-2",6"), 7.51 (2H, t, H-3",5"). ^{13}C-NMR (DMSO-*d*$_6$): δ 165.11 (C-F), 162,40 (C), 151.39 (1C, dd, $^1J_{H-F}$= 251.3 Hz, $^2J_{H-F}$= 20.0 Hz, C-F), 148.65 (1C, dd, $^1J_{H-F}$= 245.1 Hz, $^2J_{H-F}$= 16.1 Hz, C-F), 140.80 (=CH), 140.64 (1C, d, J_{H-F}= 10.3 Hz, C=N), 132.38 (2C, d, $^1J_{C-F}$= 9.1 Hz, CH-CF), 128.01 (1C, d, J_{H-F}= 12.4 Hz, C=N), 127.16 (C), 116.47 (2C, d, $^1J_{C-F}$= 22.1 Hz, CH-CF), 113.88 (C≡N), 107.09 (1C, d, $^1J_{C-F}$= 20.7 Hz, CH-CF), 99.77 (1C, d, $^1J_{C-F}$= 24.9 Hz, CH-CF). ESI-MS *m/z* calcd for $C_{15}H_7F_3N_4$ 301.06956, 302.07291, found 301.06961, 302.07288 $[M + H]^+$.

*4.5.13 (E)-3-(4-chlorophenyl)-2-(5,6-difluoro-1H-benzo[d][1,2,3]triazol-1-yl)acrylonitrile (**9g**)*
Work-up procedure (2): PS/EA 9/1. Light brown solid; $C_{15}H_7ClF_2N_4$, MW: 316.70; 34% yield (0.27 g, 0.9 mmol); m.p. 147.3-149.7 °C; R_f 0.50. ^{1}H-NMR (DMSO-*d*$_6$): δ 8.46 (1H, dd, $^1J_{H-F}$= 9.6 Hz, $^2J_{H-F}$= 7.2 Hz, H-4'), 8.36 (1H, dd, $^1J_{H-F}$= 9.6 Hz, $^2J_{H-F}$= 6.8 Hz, H-7'), 8.28 (1H, s, =CH), 8.02 (2H, d, J_{H-H}= 8.8 Hz, H-2",6"), 7.73 (2H, d, J_{H-H}= 8.8 Hz, H-3",5"). ^{13}C-NMR (DMSO-*d*$_6$): δ 151.39 (1C, dd, $^1J_{H-F}$= 249.0 Hz, $^2J_{H-F}$= 16.0 Hz, C-F), 148.69 (1C, dd, $^1J_{H-F}$= 245.0 Hz, $^2J_{H-F}$= 16.0 Hz, C-F), 140.69 (1C, d, J_{H-F}= 11.0 Hz, C=N), 140.13 (=CH), 136.49 (C), 131.38 (2CH), 129.46 (C-Cl), 129.33 (2CH), 127.91 (1C, d, J_{H-F}= 12.0 Hz, C=N), 113.69 (C≡N), 107.11 (1C, d, $^1J_{C-F}$= 20.0 Hz, CH-CF), 106.63 (C=CH), 99.85 (1C, d, $^1J_{C-F}$= 24.0 Hz, CH-CF). ESI-MS *m/z* calcd for $C_{15}H_7ClF_2N_4$ 317.04001, found 317.04178 $[M + H]^+$.

*4.5.14 (E)-3-(4-bromophenyl)-2-(5,6-difluoro-1H-benzo[d][1,2,3]triazol-1-yl)acrylonitrile (**9h**)*
Work-up procedure (2): PS/DE 8/2. White powder; $C_{15}H_7BrF_2N_4$, MW: 361.15; 47% yield (0.35 g, 1.0 mmol); m.p. 150.0-151.6 °C; R_f 0.3. ^{1}H-NMR (DMSO-*d*$_6$): δ 8.46 (1H, dd, $^1J_{H-F}$= 9.8 Hz, $^2J_{H-F}$= 7.6 Hz, H-4'), 8.37 (1H, dd, $^1J_{H-F}$= 9.6 Hz, $^2J_{H-F}$= 6.8 Hz, H-7'), 8.26 (1H, s, =CH), 7.95 (2H, d, J_{H-H}= 8.8 Hz, H-2",6"), 7.87 (2H, d, J_{H-H}= 8.4 Hz, H-3",5"). ^{13}C-NMR (DMSO-*d*$_6$): δ 151.41 (1C, dd, $^1J_{H-F}$= 250.0 Hz, $^2J_{H-F}$= 16.4 Hz, C-F), 148.67 (1C, dd, $^1J_{H-F}$= 245.0 Hz, $^2J_{H-F}$= 16.2 Hz, C-F), 140.69 (1C, d, J_{H-F}= 10.2 Hz, C=N), 140.13 (=CH), 132.20 (2CH), 131.43 (2CH), 129.75 (C), 127.85 (1C, d, J_{H-F}= 12.4 Hz, C=N), 125.43 (C-Br), 113.59 (C≡N), 107.01 (1C, d, $^1J_{C-F}$= 19.4 Hz, CH-CF), 106.67 (C=C), 99.72 (1C, d, $^1J_{C-F}$= 24.8 Hz, CH-CF). ESI-MS *m/z* $[M + H]^+$.

*4.5.15 (E)-3-(benzo[d][1,3]dioxol-4-yl)-2-(5,6-difluoro-1H-benzo[d][1,2,3]triazol-1-yl)acrylonitrile (**9i**)*
Work-up procedure (1). Yellow solid; $C_6H_8F_2N_4O_2$, MW: 326,26; 28% yield (0.13 g, 0.4 mmol); m.p. 164.6-165.2 °C; R_f 0,41. ^{1}H-NMR (DMSO-*d*$_6$): δ 8.44 (1H, dd, $^1J_{H-F}$= 9.6 Hz, $^2J_{H-F}$= 7.2 Hz, H-4'), 8.28 (1H, dd, $^1J_{H-F}$= 9.6 Hz, $^2J_{H-F}$= 6.8 Hz, H-7'), 8.15 (1H, s, =CH), 7.62 (1H, d, J_{H-H}= 1.6 Hz, H-2"), 7.56 (1H, dd, J_{H-H}= 8.4 Hz e J= 1.6 Hz, H-6"), 7.20 (1H, d, J_{H-H}= 8.4 Hz, H-5"), 6.21 (2H, s,

CH_2). ^{13}C-NMR (DMSO-d_6): δ 151.76 (1C, dd, $^1J_{H\text{-}F}$= 249.6 Hz, $^2J_{H\text{-}F}$= 16.6 Hz, C-F), 151.29 (C-O), 149.10 (1C, dd, $^1J_{H\text{-}F}$= 245.0 Hz, $^2J_{H\text{-}F}$= 16.2 Hz, C-F), 148.42 (C-O), 146.92 (=CH), 142.92 (CH), 141.06 (1C, d, $J_{H\text{-}F}$= 10.4 Hz, C=N), 128.59 (1C, d, $J_{H\text{-}F}$= 12.4 Hz, C=N), 127.52 (CH), 124.70 (C), 114.86 (C≡N), 109.49 (CH), 108.44 (CH), 107.46 (2CH, d, $^1J_{C\text{-}F}$= 28.0 Hz, CH-CF), 103.68 (C=CH), 102.73 (O-CH_2-O), 99.96 (2CH, d, $^1J_{C\text{-}F}$= 24.8 Hz, CH-CF). ESI-MS *m/z* calcd for $C_{16}H_8F_2N_4O_2$ 327.06881, 328.07216, found 327.06906, 328.07233 $[M + H]^+$.

*4.5.16 (E)-2-(5,6-difluoro-1H-benzo[d][1,2,3]triazol-1-yl)-3-(isoquinolin-5-yl)acrylonitrile (**9j**)*
Work-up procedure (1). Light brown solid; $C_{18}H_9F_2N_5$, MW: 333.30; 33% yield (0.2 g, 0.6 mmol); m.p. 109.4-111.5 °C; R_f 0.10. ^{1}H-NMR (DMSO-d_6): δ 9.47 (1H, s, H-1"), 8.91 (1H, s, =CH), 8.64 (1H, d, $J_{H\text{-}H}$= 6 Hz, H-3"), 8.49 (1H, d, $J_{H\text{-}H}$= 7.2 Hz, H-8"), 8.44 (2H, m, H-4',7'), 8.39 (1H, d, $J_{H\text{-}H}$= 8.4 Hz, H-6"), 8.12 (1H, d, $J_{H\text{-}H}$= 6.0 Hz, H-4"), 7.93 (1H, t, $J_{H\text{-}H}$= 7.8 Hz, H-7"). ^{13}C-NMR (DMSO-d_6): δ 153.05 (CH), 151.43 (1C, dd, $^1J_{H\text{-}F}$= 249.0 Hz, $^2J_{H\text{-}F}$= 16.0 Hz, C-F), 148.68 (1C, dd, $^1J_{H\text{-}F}$= 245.0 Hz, $^2J_{H\text{-}F}$= 16.0 Hz, C-F), 144.03 (CH), 140.73 (1C, d, $J_{c\text{-}F}$= 11.0 Hz, C=N), 138.08 (CH), 133.64 (C=CH), 131.45 (CH), 131.23 (CH), 128.18 (1C, d, $J_{c\text{-}F}$= 13.0 Hz, C=N), 128.06 (C), 127.50 (C), 127.17 (=CH), 117.25 (CH), 113.42 (C≡N), 109.82 (C), 107.07 (2CH, d, $^1J_{C\text{-}F}$= 21.0 Hz, CH-CF), 100.16 (2CH, d, $^1J_{C\text{-}F}$= 25.0 Hz, CH-CF). ESI-MS *m/z* calcd for $C_{18}H_9F_2N_5$ 334.08988, 335.09323, 336.09659, found 334.09045, 335.09366, 336.09689 $[M + H]^+$.

*4.5.17 (Z)-2-(5,6-difluoro-1H-benzo[d][1,2,3]triazol-1-yl)-3-(4-nitrophenyl)acrylonitrile (**10e**)*
Work-up procedure (1). Red solid; $C_{15}H_7F_2N_5O_2$, MW: 327.25; 26% yield (0.12 g, 0.4 mmol); m.p. 179.3-181.2 °C; R_f 0,68. ^{1}H-NMR (DMSO-d_6): δ 8.53 (1H, dd, $^1J_{H\text{-}F}$= 10.0 Hz, $^2J_{H\text{-}F}$= 7.2 Hz, H-4'), 8.32 (2H, d, $J_{H\text{-}H}$= 8.8 Hz, H-3",5"), 7.74 (1H, dd, $^1J_{H\text{-}F}$= 9.6 Hz, $^2J_{H\text{-}F}$= 6.8 Hz, H-7'), 7.69 (2H, d, $J_{H\text{-}H}$= 8.8 Hz, H-2",6"), 7.27 (1H, s, =CH). ^{13}C-NMR (DMSO-d_6): δ 151.34 (1C, dd, $^1J_{C\text{-}F}$= 250.5 Hz, $^2J_{C\text{-}F}$= 16.0 Hz, C-F), 149.45 (C-NO_2), 148.70 (1C, dd, $^1J_{C\text{-}F}$= 227.5 Hz, $^2J_{C\text{-}F}$= 16.0 Hz, C-F), 147.63 (C), 140.59 (1C, d, $J_{H\text{-}F}$= 10.0 Hz, C=N), 137.20 (C=CH), 129.19 (2CH), 124.18 (1C, d, $J_{H\text{-}F}$= 17.0 Hz, C=N), 124.26 (2CH), 114.83 (C≡N), 107.43 (2CH, d, $^1J_{C\text{-}F}$= 20.0 Hz, CH-CF), 99.77 (1C, d, $^1J_{C\text{-}F}$= 25.0 Hz, CH-CF), 99.64 (=CH). ESI-MS *m/z* calcd for $C_{18}H_9F_2N_5$ 311.06467, found 311.25558 $[M + H]^+$.

*4.5.18 (E)-2-(5,6-difluoro-2H-benzo[d][1,2,3]triazol-2-yl)-3-(p-tolyl)acrylonitrile (**11a**)*
Work-up procedure (1). Yellow solid; $C_{16}H_{10}F_2N_4$, MW: 296,28; 42% yield (0.16 g, 0.5 mmol); m.p. 158.1-160.5 °C; R_f 0,83. ^{1}H-NMR (DMSO-d_6): δ 8.66 (1H, s, =CH), 8.23 (2H, t, $^1J_{H\text{-}H}$= 8.8 Hz, H-4',7'), 7.96 (2H, d, $J_{H\text{-}H}$= 8.0 Hz, H-2",6"), 7.44 (2H, d, $J_{H\text{-}H}$= 8.0 Hz, H-3",5"), 2.42 (3H, s, CH_3). ^{13}C-NMR (DMSO-d_6): δ 151.39 (2C, dd, $^1J_{C\text{-}F}$= 250.5 Hz, $^2J_{C\text{-}F}$= 19.0 Hz, C-F), 142.87 (2C, t, $^1J_{C\text{-}F}$= 7.0 Hz, C=N), 138.24 (C=CH), 130.00 (2CH), 129.96 (2CH), 127.27 (C), 113.08 (C≡N), 110.45 (C=CH), 104.33 (2CH, m, CH-CF), 21.23 (CH_3). ESI-MS *m/z* calcd for $C_{16}H_{10}F_2N_4$ 297.09463, found 297.09482 $[M + H]^+$.

*4.5.19 (E)-2-(5,6-difluoro-2H-benzo[d][1,2,3]triazol-2-yl)-3-(4-methoxyphenyl)acrylonitrile (**11b**)*
Work-up procedure (1). Brown solid; $C_{16}H_{10}F_2N_4O$, MW: 312,28; 39% yield (0.17 g, mmol); m.p. 148.6-149.3 °C; R_f 0,43. ^{1}H-NMR (DMSO-d_6): δ 8.62 (1H, s, =CH), 8.21 (2H, t, $^1J_{H\text{-}H}$= 8.8 Hz, H-4',7'), 8.06 (2H, d, $J_{H\text{-}H}$= 8.8 Hz, H-2",6"), 7.18 (2H, d, $J_{H\text{-}H}$= 8.8 Hz, H-3",5"), 3.88 (3H, s, OCH_3). ^{13}C-NMR (DMSO-d_6): δ 162.52 (C-OCH_3), 151.27 (2C, dd, $^1J_{C\text{-}F}$= 250.5 Hz, $^2J_{C\text{-}F}$= 20.0 Hz, C-F), 140.37 (2C, t, $^1J_{C\text{-}F}$= 6.0 Hz, C=N), 138.07 (C=CH), 132.23 (2CH), 122.32 (C), 114.97 (2CH), 113.43

(C≡N), 108.68 (C=CH), 104.24 (2CH, m, CH-CF), 55.64 (CH_3). ESI-MS *m/z* calcd for $C_{16}H_{10}F_2N_4O$ 313.08954, found 313.08975 $[M + H]^+$.

*4.5.20 (E)-2-(1H-benzo[d][1,2,3]triazol-1-yl)-3-(4-hydroxyphenyl)acrylonitrile (**13d**)*
Work-up procedure (2): $CHCl_3/CH_3OH$ 9.9/0.1. Yellow solid; $C_{15}H_{10}N_4O$, MW: 262.27; 28% yield (0.2 g, 0.8 mmol); m.p. 115.4-116.5 °C; R_f 0.38. ^{1}H-NMR (DMSO-d_6): δ 8.22 (2H, d, $^1J_{H-H}$= 8.4 Hz, H-4'), 8.12 (1H, s, =CH), 7.98 (1H, d, J_{H-H}= 8.4 Hz, H-7'), 7.93 (2H, d, J_{H-H}= 8.4 Hz, H-2",6"), 7.73 (1H, d, J_{H-H}= 7.8 Hz, H-6'), 7.00 (2H, d, J_{H-H}= 8.4 Hz, H-3",5"). ^{13}C-NMR (DMSO-d_6): δ 161.86 (C-OH), 145.71 (C=N), 143.31 (CH), 132.61 (2CH), 132.29 (C=N), 129.63 (CH), 125.68 (CH), 121.75 (C-CH), 120.35 (CH), 116.73 (2CH), 115.39 (C≡N), 111.30 (CH), 102.06 (C). ESI-MS *m/z* calcd for $C_{15}H_{10}N_4O$ 263.09274, found 263.53491 $[M - H]^-$.

*4.5.21 (E)-2-(1H-benzo[d][1,2,3]triazol-1-yl)-3-(isoquinolin-5-yl)acrylonitrile (**13j**)*
Work-up procedure (1). Brick red-brown powder. $C_{18}H_{11}N_5$, MW: 297.32; 35% yield (0.23 g, 0.8 mmol); m.p. 131.4 – 133.3 °C; R_f 0.04. ^{1}H-NMR (DMSO-d_6): δ 9.47 (1H, s, H-1"), 8.92 (1H, s, =CH), 8.63 (1H, d, J_{H-H}= 5.6 Hz, H-3"), 8.50 (1H, d, J_{H-H}= 7.2 Hz, H-4'), 8.39 (1H, d, J_{H-H}= 8.0 Hz, H-4"), 8.28 (1H, d, J_{H-H}= 8.4 Hz, H-8"), 8.18 (1H, d, J_{H-H}= 8.4 Hz, H-7'), 8.14 (1H, d, J_{H-H}= 6 Hz, H-6"), 7.93 (1H, t, J_{H-H}= 8.0 Hz, H-6'), 7.79 (1H, t, J_{H-H}= 8.0 Hz, H-7"), 7.62 (1H, t, J_{H-H}= 8.0 Hz, H-5').^{13}C-NMR (DMSO-d_6): δ 153.05 (CH=N isoq), 145.49 (C=N), 144.06 (CH=N isoq), 137.02 (CH), 133.65 (C=CH), 131.62 (C=N), 131.41 (CH), 131.09 (CH), 129.44 (CH), 128.09 (C), 127.60 (C), 127.20 (CH), 125.53 (CH), 119.99 (=CH), 117.20 (CH), 113.53 (CN), 111.51 (CH), 110.34 (C). ESI-MS *m/z* calcd for $C_{15}H_{10}N_4O$, found 263.06778, 264.07114 $[M + H]^+$.

5. Acknowledgments

We acknowledge “Assessorato della Programmazione, Bilancio, Credito e Assetto del territorio” of “Regione Autonoma della Sardegna” (Sardinia, Italy) for the funding support with the grant named “Legge Regionale 7 agosto 2007:CRP1_574, 22/41 del 2017”, grant number RASSR01499. F.R. acknowledges MIUR (Ministero dell’Istruzione, dell’Università e della Ricerca) for the PhD grant. We thank the National Cancer Institute, Developmental Therapeutics Program, NCI (Bethesda, MD, USA; https://dtp.cancer.gov) as the source of the data from *in vitro* anti-cancer screening. We acknowledge Kitos Biotech for *in vitro* **9a**-EPI combination assay. F.R acknowledges the Erasmus+ program. F.R. thanks Prof. Göran Widmalm and Alessandro Ruda, for the support during his PhD Erasmus+ at the Stockholm University, Sweden. We acknowledge Schrödinger® for the short term free license for Maestro package.

6. Author Contributions

Conceptualisation, F.R., R.I., S.P. and A.C.; formal analysis, F.R., R.I., V.B., L.S., M.A.S. and M.L.; investigation, F.R., R.I., V.B., L.S., M.A.S. and M.L.; resources, A.C.; data curation, F.R., R.I., V.B., L.S., M.A.S., M.L., L.B. and A.C.; writing/original draft preparation, F.R., R.I.; writing/review and editing, all authors; visualization, F.R., R.I. and A.C.; supervision, L.B., A.C., funding acquisition, L.B., A.C. All authors have read and agreed to the published version of the manuscript.

7. Conflict of interest

The authors declare that the research was conducted in the absence of any commercial or financial relationships that could be construed as a potential conflict of interest.

8. References

[1] F. Bray, J. Ferlay, I. Soerjomataram, R.L. Siegel, L.A. Torre, A. Jemal, Global cancer statistics 2018: GLOBOCAN estimates of incidence and mortality worldwide for 36 cancers in 185 countries., CA. Cancer J. Clin. 68 (2018) 394–424. https://doi.org/10.3322/caac.21492.

[2] A. Damasceno, Noncommunicable Disease, 2016. https://doi.org/10.1002/9781119097136.part5.

[3] G. Bérubé, How to utilize academic research efforts in cancer drug discovery, Expert Opin. Drug Discov. 14 (2019) 331–334. https://doi.org/10.1080/17460441.2019.1582637.

[4] Y. Imoto, Y. Yoshida, F. Yagisawa, H. Kuroiwa, T. Kuroiwa, The cell cycle, including the mitotic cycle and organelle division cycles, as revealed by cytological observations, J. Electron Microsc. (Tokyo). 60 (2011) 117–136. https://doi.org/10.1093/jmicro/dfr034.

[5] S. Florian, T.J. Mitchison, Anti-microtubule drugs, Methods Mol. Biol. 1413 (2016) 403–421. https://doi.org/10.1007/978-1-4939-3542-0_25.

[6] G. Chandrasekaran, P. Tátrai, F. Gergely, Hitting the brakes: Targeting microtubule motors in cancer, Br. J. Cancer. 113 (2015) 693–698. https://doi.org/10.1038/bjc.2015.264.

[7] E. Mukhtar, V.M. Adhami, H. Mukhtar, Targeting microtubules by natural agents for cancer therapy, Mol. Cancer Ther. 13 (2014) 275–284. https://doi.org/10.1158/1535-7163.MCT-13-0791.

[8] A. Massarotti, A. Coluccia, R. Silvestri, G. Sorba, A. Brancale, The tubulin colchicine domain: A molecular modeling perspective, ChemMedChem. 7 (2012) 33–42. https://doi.org/10.1002/cmdc.201100361.

[9] Y. Lu, J. Chen, M. Xiao, W. Li, D.D. Miller, An overview of tubulin inhibitors that interact with the colchicine binding site, Pharm. Res. 29 (2012) 2943–2971. https://doi.org/10.1007/s11095-012-0828-z.

[10] A.M. Tsimberidou, W. Akerley, M.C. Schabel, D.S. Hong, C. Uehara, A. Chhabra, T. Warren, G.G. Mather, B.A. Evans, D.P. Woodland, E.A. Swabb, R. Kurzrock, Phase I clinical trial of MPC-6827 (Azixa), a microtubule destabilizing agent, in patients with advanced cancer, Mol. Cancer Ther. 9 (2010) 3410–3419. https://doi.org/10.1158/1535-7163.MCT-10-0516.

[11] J.Y. Bruce, J. Eickhoff, R. Pili, T. Logan, M. Carducci, J. Arnott, A. Treston, G. Wilding, G. Liu, A phase II study of 2-methoxyestradiol nanocrystal colloidal dispersion alone and in combination with sunitinib malate in patients with metastatic renal cell carcinoma progressing on sunitinib malate, Invest. New Drugs. 30 (2012) 794–802. https://doi.org/10.1007/s10637-010-9618-9.

[12] P. Liu, Y. Qin, L. Wu, S. Yang, N. Li, H. Wang, H. Xu, K. Sun, S. Zhang, X. Han, Y. Sun, Y. Shi, A phase i clinical trial assessing the safety and tolerability of combretastatin A4 phosphate injections, Anticancer. Drugs. 25 (2014) 462–471. https://doi.org/10.1097/CAD.0000000000000070.

[13] D.M. Patterson, M. Zweifel, M.R. Middleton, P.M. Price, L.K. Folkes, M.R.L. Stratford, P. Ross, S. Halford, J. Peters, J. Balkissoon, D.J. Chaplin, A.R. Padhani, G.J.S. Rustin, Phase I clinical and pharmacokinetic evaluation of the vascular-disrupting agent OXi4503 in patients with advanced solid tumors, Clin. Cancer Res. 18 (2012) 1415–1425. https://doi.org/10.1158/1078-0432.CCR-11-2414.

[14] P. Sanna, A. Carta, L. Gherardini, Synthesis and antimycobacterial activity of 3-aryl- , 3-cyclohexyl- and 3-heteroaryl-, 57 (2002) 79–87.

[15] A. Carta, P. Sanna, M. Palomba, L. Vargiu, M. La Colla, R. Loddo, Synthesis and antiproliferative activity of 3-aryl-2-(1H-benzotriazol-1-yl)acrylonitriles. Part III, Eur. J. Med. Chem. 37 (2003) 891–900. https://doi.org/10.1016/S0223-5234(02)01411-3.
[16] A. Carta, M. Palomba, G. Boatto, B. Busonera, M. Murreddu, R. Loddo, Synthesis and antiproliferative activity of 3-aryl-2-[1H(2H)-benzotriazol- 1(2)-yl]acrylonitriles variously substituted: Part 4, Farmaco. 59 (2004) 637–644. https://doi.org/10.1016/j.farmac.2004.03.004.
[17] A. Carta, I. Briguglio, S. Piras, G. Boatto, P. La Colla, R. Loddo, M. Tolomeo, S. Grimaudo, A. Di Cristina, R.M. Pipitone, E. Laurini, M.S. Paneni, P. Posocco, M. Fermeglia, S. Pricl, 3-Aryl-2-[1H-benzotriazol-1-yl]acrylonitriles: A novel class of potent tubulin inhibitors, Eur. J. Med. Chem. 46 (2011) 4151–4167. https://doi.org/10.1016/j.ejmech.2011.06.018.
[18] I. Briguglio, E. Laurini, M.A. Pirisi, S. Piras, P. Corona, M. Fermeglia, S. Pricl, A. Carta, Triazolopyridinyl-acrylonitrile derivatives as antimicrotubule agents: Synthesis, in vitro and in silico characterization of antiproliferative activity, inhibition of tubulin polymerization and binding thermodynamics, Eur. J. Med. Chem. 141 (2017) 460–472. https://doi.org/10.1016/j.ejmech.2017.09.065.
[19] P. Sanna, A. Carta, M.E.R. Nikookar, Synthesis and antitubercular activity of 3-aryl substituted-2-(1H(2H) benzotriazol-1(2)-yl)acrylonitriles, Eur. J. Med. Chem. 35 (2000) 535–543. https://doi.org/10.1016/S0223-5234(00)00144-6.
[20] H. van de W. and D.K.W. D. A. Smith, Methods and Principles in Medicinal Chemistry, vol. 31: Pharmacokinetics and Metabolism in Drug Design, , Wiley-VCH, Weinheim, 2006.
[21] B.E. Smart, Fluorine substituent effects (on bioactivity), J. Fluor. Chem. 109 (2001) 3–11. https://doi.org/10.1016/S0022-1139(01)00375-X.
[22] S. Purser, P.R. Moore, S. Swallow, V. Gouverneur, Fluorine in medicinal chemistry, Chem. Soc. Rev. 37 (2008) 320–330. https://doi.org/10.1039/b610213c.
[23] The PyMOL Molecular Graphics System, Version 2.0 Schrödinger, LLC., (n.d.).
[24] Maestro, version 10.2, Schrödinger, LLC, New York, NY, 2015., (n.d.).
[25] L. RA, S. MB, LigPlot+: multiple ligand-protein interaction diagrams for drug discovery, J. Chem. Inf. Model. 51 (2011) 2778–2786.
[26] K. Eskandari, M. Lesani, Does fluorine participate in halogen bonding?, Chem. - A Eur. J. 21 (2015) 4739–4746. https://doi.org/10.1002/chem.201405054.
[27] A.J. Morris, G. M., Huey, R., Lindstrom, W., Sanner, M. F., Belew, R. K., Goodsell, D. S. and Olson, AutoDock4 and AutoDockTools4: Automated Docking with Selective Receptor Flexibility, J. Comput. Chem. 16 (2009) 2785–91.
[28] C.S. See, M. Kitagawa, P.J. Liao, K.H. Lee, J. Wong, S.H. Lee, B.W. Dymock, Discovery of the cancer cell selective dual acting anti-cancer agent (Z)-2-(1H-indol-3-yl)-3-(isoquinolin-5-yl)acrylonitrile (A131), Eur. J. Med. Chem. 156 (2018) 344–367. https://doi.org/10.1016/j.ejmech.2018.07.011.
[29] L. Sanna, R. Piredda, I. Marchesi, V. Bordoni, S.V. Forcales, D.F. Calvisi, L. Bagella, “Verteporfin exhibits anti-proliferative activity in embryonal and alveolar rhabdomyosarcoma cell lines”, Chem. Biol. Interact. 312 (2019) 108813. https://doi.org/10.1016/j.cbi.2019.108813.
[30] J. Barretina, G. Caponigro, N. Stransky, K. Venkatesan, A.A. Margolin, S. Kim, C.J. Wilson, J. Lehár, G. V. Kryukov, D. Sonkin, A. Reddy, M. Liu, L. Murray, M.F. Berger, J.E. Monahan, P. Morais, J. Meltzer, A. Korejwa, J. Jané-Valbuena, F.A. Mapa, J. Thibault, E. Bric-Furlong, P. Raman, A. Shipway, I.H. Engels, J. Cheng, G.K. Yu, J. Yu, P. Aspesi, M. De Silva, K. Jagtap, M.D. Jones, L. Wang, C. Hatton, E. Palescandolo, S. Gupta, S. Mahan, C. Sougnez, R.C. Onofrio, T. Liefeld, L. MacConaill, W. Winckler, M. Reich, N. Li, J.P. Mesirov, S.B. Gabriel, G. Getz, K. Ardlie, V. Chan, V.E. Myer, B.L. Weber, J. Porter, M. Warmuth, P. Finan, J.L. Harris, M. Meyerson, T.R. Golub, M.P. Morrissey, W.R. Sellers, R. Schlegel, L.A. Garraway, The Cancer Cell Line Encyclopedia enables predictive modelling

of anticancer drug sensitivity, Nature. 483 (2012) 603–607. https://doi.org/10.1038/nature11003.
[31] O.A.J. Trott, O., AutoDock Vina: Improving the Speed and Accuracy of Docking with a New Scoring Function, Efficient Optimization, and Multithreading, J. Comput. Chem. 31 (2010) 455–461. https://doi.org/10.1002/jcc.21334.
[32] Z. Wang, H. Sun, X. Yao, D. Li, L. Xu, Y. Li, S. Tian, T. Hou, Comprehensive evaluation of ten docking programs on a diverse set of protein-ligand complexes: The prediction accuracy of sampling power and scoring power, Phys. Chem. Chem. Phys. 18 (2016) 12964–12975. https://doi.org/10.1039/c6cp01555g.
[33] H.M. Berman, T. Battistuz, T.N. Bhat, W.F. Bluhm, P.E. Bourne, K. Burkhardt, Z. Feng, G.L. Gilliland, L. Iype, S. Jain, P. Fagan, J. Marvin, D. Padilla, V. Ravichandran, B. Schneider, N. Thanki, H. Weissig, J.D. Westbrook, C. Zardecki, The protein data bank, Acta Crystallogr. Sect. D Biol. Crystallogr. 58 (2002) 899–907. https://doi.org/10.1107/S0907444902003451.
[34] K. Stott, J. Keeler, Q.N. Van, A.J. Shaka, One-Dimensional NOE Experiments Using Pulsed Field Gradients, J. Magn. Reson. 125 (1997) 302–324. https://doi.org/10.1006/jmre.1997.1110.
[35] Y. Binev, M.M.B. Marques, J. Aires-de-Sousa, Prediction of1H NMR coupling constants with associative neural networks trained for chemical shifts, J. Chem. Inf. Model. 47 (2007) 2089–2097. https://doi.org/10.1021/ci700172n.
[36] C.A. Lipinski, F. Lombardo, B.W. Dominy, P.J. Feeney, Experimental and computational approaches to estimate solubility and permeability in drug discovery and development settings, Adv. Drug Deliv. Rev. (2012). https://doi.org/10.1016/j.addr.2012.09.019.
[37] R.J. Faggyas, N.L. Sloan, N. Buijs, A. Sutherland, Synthesis of Structurally Diverse Benzotriazoles via Rapid Diazotization and Intramolecular Cyclization of 1,2-Aryldiamines, European J. Org. Chem. 2019 (2019) 5344–5353. https://doi.org/10.1002/ejoc.201900463.